HHS Public Access

Author manuscript

Chem Biol Drug Des. Author manuscript; available in PMC 2021 June 01.

Published in final edited form as:

Chem Biol Drug Des. 2021 May ; 97(5): 1059–1078. doi:10.1111/cbdd.13826.

Design and synthesis of isothiocyanate-containing hybrid androgen receptor (AR) antagonist to downregulate AR and induce ferroptosis in GSH–Deficient prostate cancer cells

Zhihui Qin[1], **Siyu Ou**[1], **Liping Xu**[1], **Kathleen Sorensen**[1], **Yingxue Zhang**[2], **Dan-Ping Hu**[3], **Zhe Yang**[2], **Wen-Yang Hu**[3], **Fei Chen**[1], **Gail S. Prins**[3]

[1]Department of Pharmaceutical Sciences, Eugene Applebaum College of Pharmacy and Health Sciences, Wayne State University, Detroit, MI, USA

[2]Department of Biochemistry, Microbiology and Immunology, Wayne State University School of Medicine, Detroit, MI, USA

[3]Department of Urology, University of Illinois at Chicago, Chicago, IL, USA

Abstract

Sustained androgen receptor (AR) signaling and apoptosis evasion are among the main hurdles of castration-resistant prostate cancer (CRPC) treatment. We designed and synthesized isothiocyanate (ITC)-containing hybrid AR antagonist (ITC-ARi) and rationally combined ITC-ARi with GSH synthesis inhibitor buthionine sulfoximine (BSO) to efficiently downregulate AR/AR splice variant and induce ferroptosis in CRPC cells. The representative ITC-ARi **13** is an AR ligand that contains an *N*-acetyl cysteine-masked ITC moiety and gradually releases parental unconjugated ITC **12b** in aqueous solution. The in vitro anti-PCa activities of **13**, such as growth inhibition and AR downregulation, are significantly enhanced when combined with BSO. The drug combination caused notable lipid peroxidation and the cell viability was effectively rescued by iron chelator, antioxidants or the inhibitor of heme oxygenase-1, supporting the induction of ferroptosis. **13** and BSO cooperatively downregulate AR and induce ferroptosis likely through increasing the accessibility of **13**/**12b** to cellular targets, escalating free intracellular ferrous iron and attenuating GSH-centered cellular defense and adaptation. Further studies on the combination of ITC-ARi and GSH synthesis inhibitor could result in a new modality against CRPC.

Keywords

androgen receptor; androgen receptor splice variant 7; BSO; castration-resistant prostate cancer; drug combination; ferroptosis; GSH; hybrid androgen receptor antagonist; hybrid drug; isothiocyanate

Correspondence Zhihui Qin, Department of Pharmaceutical Sciences, Eugene Applebaum College of Pharmacy and Health Sciences, Wayne State University, 259 Mack Ave., Detroit, MI 48201, USA, zqin@wayne.edu.

CONFLICT OF INTEREST

Z.Q and L.X. are inventors of a patent application filed by WSU for the use of ITC-ARi in combination with BSO as anticancer agents.

SUPPORTING INFORMATION

Additional supporting information may be found online in the Supporting Information section.

1 | INTRODUCTION

Prostate cancer (PCa) is the most common male malignancy with about 170,000 new cases and 30,000 deaths in United States in 2019. Although androgen deprivation therapy (ADT) is available as a standard care, PCa could still progress to a fatal stage termed castration-resistant prostate cancer (CRPC) within 2–3 years of ADT (Harris et al., 2009). Because of persistent androgen receptor (AR) signaling in CRPC, novel androgen biosynthesis inhibitor abiraterone and AR antagonist (ARi) enzalutamide (Enz, Figure 1a) were developed. However, intrinsic and acquired resistance inevitably lead to variable response and short-lived survival benefits. Numerous mechanisms contribute to AR re-activation in CRPC, such as: AR amplification and overexpression (Haapala et al., 2007) enabling CRPC respond to low levels of androgen; AR mutations allowing promiscuous receptor activation by alternative ligands (Korpal et al., 2013) and the expression of AR splice variants (AR-Vs) without ligand-binding domain (LBD). AR-Vs are constitutively active and cannot be inhibited by conventional ARis (e.g., Enz) or by androgen biosynthesis inhibitors (e.g., abiraterone) (Li et al., 2013).

Isothiocyanates (ITCs), such as phenethyl isothiocyanate (PEITC) and sulforaphane (SFN) (Figure 1a), are bioactive metabolites of naturally occurring glucosinolates existing in cruciferous vegetables. Dietary intake of ITCs decreases the incidence of PCa (Traka et al., 2014). In recurrent patients, SFN-enriched broccoli sprout extract prolonged doubling time of prostate-specific antigen, further indicating the therapeutic potential of ITC in CRPC (Alumkal et al., 2015). ITCs are inhibitory to multiple PCa growth and survival mechanisms, for example, PEITC accelerates AR degradation (Wang et al., 2006); SFN-*N*-acetyl cysteine (NAC) conjugate inhibits histone deacetylase (HDAC) 6 and therefore disrupts the interaction of AR with heat shock protein (Hsp) 90 (Gibbs et al., 2009). ITCs also downregulate antiapoptotic proteins (Hwang & Lee, 2010) in PCa cells and suppress PCa stem-like cells (Vyas et al., 2016).

To address the challenges of CRPC treatment, we designed isothiocyanate (ITC)-containing AR antagonists (ITC-ARis) by incorporating ITC moiety into the chemical scaffold of an ARi (Figure 1a) (Ou et al., 2017; Qin et al., 2019). The chemical simplicity of ITC allows dual-pharmacophore hybrid drug design without significantly disrupting AR affinity. As a single-molecule AR-targeting agent, we envisioned that ITC-ARi antagonistically binds to full-length AR (FL AR) and meanwhile possesses ITC-derived polypharmacological anti-PCa activities, including the downregulation of AR. Compared to the parental ARi and ITC, this hybrid drug approach efficiently co-localizes ARi and anti-PCa properties of ITC in the same cell and as shown in this work, is highly feasible in the development of combinatorial anti-PCa treatments.

Ferroptosis is a regulated non-apoptotic cell death caused by reactive oxygen species (ROS) and iron-dependent lipid peroxidation (Stockwell et al., 2017). Growing evidences support the exploitation of ferroptosis as a new anticancer approach (Zhang et al., 2019). Across diverse cancer types, treatment-resistant cancer cell populations (Viswanathan et al., 2017), such as persister cells (Hangauer et al., 2017) and cancer stem cells (Mai et al., 2017), are susceptible to ferroptosis induction. Since treating hormone-refractory PCa is hurdled by

apoptosis evasion (McKenzie & Kyprianou, 2006), ferroptosis-inducing therapies could be of high value for CRPC patients. Here, we report the design, synthesis of ITC-ARi **13** and its polypharmacological in vitro anti-PCa activities, either alone or in combination with GSH synthesis inhibitor buthionine sulfoximine (BSO). **13** antagonizes AR transactivation and downregulates AR/AR-V7 expression. The combination of **13** and BSO further causes ferroptosis in Enz-resistant PCa cells, supporting the combination of ITC-ARi and GSH synthesis inhibitor as potential therapies against CRPC.

2 | METHODS AND MATERIALS

2.1 | Chemistry

2.1.1 | General methods—All reagents and solvents were purchased from commercial suppliers and used without further purification. The reactions were monitored by using thin-layer chromatography (TLC) on precoated silica gel UV254 plates (Sorbtech) and visualized under UV light or after staining by dipping into a solution of phosphomolybdic acid or potassium permanganate and then heated on a hot plate. All the final compounds were purified to > 95% purity by performing flash column chromatography over 200–300 mesh silica gel, and further determined by using high-performance liquid chromatography (HPLC). All NMR spectra were obtained using Bruker Ascend™−400 or Varian INOVA 600 MHz NMR spectrometer. Chemical shifts are expressed in ppm as a δ value, and singlet (s), doublet (d), triplet (t), quartet (q), multiplet (m), and broad singlet (bs) are used as abbreviations. High resolution mass spectroscopy (HRMS) was collected by using a LCT Premier XE KD128 instrument. Low-resolution mass spectroscopy was collected by using an Advion expression^{L} compact mass spectrometers instrument. HPLC analysis was conducted using a Phenomenex (Luna^{R}) C18 (3.5 μm), 3.0 mm × 100 mm column on a Agilent 1100 instrument. Two solvents were used: solvent A, water containing 0.1% formic acid (FA) and 10% (v/v) CH_3OH; solvent B, 0.1% FA in CH_3CN. Flow rate was set at 0.5 ml/min.

2.1.2 | General procedure for the synthesis of ITC-ARi 12a, 12b, and 13

***4-(5-Nitropyridin-2-yl)but-3-yn-1-ol* (3a):** In argon atmosphere, to a mixture of 2-bromo-5-nitropyridine (10.0 g, 49 mmol) and 3-butyn-1-ol (4.55 g, 65 mmol) in acetonitrile (70 ml) were added copper iodide (190 mg, 1 mmol), bis(triphenylphosphine) palladium (II) chloride (175 mg, 0.25 mmol). Triethylamine (TEA) (34 ml, 250 mmol) was slowly added with stirring at 0°C. The mixture was stirred at room temperature overnight. Solvent was removed under reduced pressure. The residue was diluted with EtOAc and was washed with water and brine. The organic phase was separated and dried over anhydrous Na_2SO_4 and concentrated. The crude product was purified by using flash column chromatography (Hexanes/EtOAc: 1:1) to afford **3a** as brown oil (8.34 g, 87%). ^{1}H NMR (600 MHz, $CDCl_3$) δ 9.36 (d, J = 2.3 Hz, 1H), 8.42 (dd, J = 8.6 Hz, 2.3 Hz, 1H), 7.57 (d, J = 8.6 Hz, 1H), 3.90 (t, J = 6.1 Hz, 2H), 2.86 (bs, 1H), 2.78 (t, J = 6.2 Hz, 2H). ^{13}C-NMR (100 MHz, $CDCl_3$): δ 148.70, 145.27, 142.64, 131.43, 126.89, 94.25, 80.91, 60.46, 23.98.

***6-(5-Nitropyridin-2-yl)hex-5-yn-1-ol* (3b):** **3b** was prepared similarly as described for **3a**. 2-bromo-5-nitropyridine (13.2 g, 65 mmol) and 5-hexyn-1-ol (4.9 g, 50 mmol) were used for

this reaction. The crude product was purified by using flash column chromatography (Hexanes/EtOAc: 2:1) to afford **3b** as brown oil (10.5 g, 95%). ^{1}H NMR (400 MHz, $CDCl_3$): δ 9.35 (d, J = 2.4 Hz, 1H), 8.42 (dd, J = 8.6 Hz, 2.6 Hz, 1H), 7.54 (d, J = 8.6 Hz, 1H), 3.72 (t, J = 5.7 Hz, 2H), 2.54 (t, J = 6.5 Hz, 2H), 1.87 (bs, 1H), 1.75–1.79 (m, 4H). ^{13}C NMR (100 MHz, $CDCl_3$): δ 149.15, 145.30, 142.48, 131.27, 126.77, 97.22, 80.10, 62.20, 31.84, 24.44, 19.40.

***2-(4-(Methoxymethoxy)but-1-yn-1-yl)-5-nitropyridine* (4a):** In argon atmosphere, to a solution of **3a** (8.34 g, 43.4 mmol) in THF (80 ml) were added *N,N*-diisopropylethylamine (DIPEA; 18 ml, 108.6 mmol). Bromo(methoxy)methane (7.2 ml, 90%, 78 mmol) was then slowly added at 0°C. Reaction was stirred at room temperature overnight. Precipitate was filtered and filtrate was evaporated under reduced pressure. The residue was diluted with EtOAc and was washed with water and brine. The organic phase was separated and dried over anhydrous Na_2SO_4 and concentrated. The crude product was purified by using flash column chromatography (Hexanes/EtOAc: 6:1 → 4:1) to afford **4a** as yellow solid (6.3 g, 61%). ^{1}H NMR (400 MHz, $CDCl_3$): δ 9.36 (d, J = 2.6 Hz, 1H), 8.43 (dd, J = 8.6 Hz, 2.6 Hz, 1H), 7.56 (d, J = 8.6 Hz, 1H), 4.68 (s, 2H), 3.80 (t, J = 6.7 Hz, 2H), 3.40 (s, 3H), 2.82 (t, J = 6.7 Hz, 2H). ^{13}C-NMR (100 MHz, CDCl3): 148.87, 145.31, 142.59, 131.27, 126.88, 96.50, 93.96, 80.47, 65.23, 55.40, 21.17.

***2-(6-(Methoxymethoxy)hex-1-yn-1-yl)-5-nitropyridine* (4b):** **4b** was prepared similarly as described for **4a** by using **3b** (10.5 g, 47.7 mmol) as the starting material. The crude product was purified by using flash column chromatography (Hexanes/EtOAc: 4:1) to afford **4b** as brown oil (10.69 g, 85%). ^{1}H NMR (400 MHz, $CDCl_3$): δ 9.36 (d, J = 2.6 Hz, 1H), 8.42 (dd, J = 8.6 Hz, 2.7 Hz, 1H), 7.53 (d, J = 8.6 Hz, 1H), 4.63 (s, 2H), 3.58 (t, J = 5.4 Hz, 2H), 3.37 (s, 3H), 2.56 (t, J = 6.4 Hz, 2H), 1.75–1.80 (m, 4H). ^{13}C NMR (100 MHz, $CDCl_3$): δ 149.20, 145.31, 142.47, 131.22, 126.77, 97.15, 96.48, 80.07, 67.07, 55.20, 29.02, 24.94, 19.40.

***6-(4-(Methoxymethoxy)butyl)pyridin-3-amine* (5a):** Palladium on carbon (200 mg) was added to a solution of **4a** (8.40 g, 35.6 mmol) in methanol (100 ml). The reaction was stirred at pressurized hydrogen atmosphere (60 psi) overnight. The mixture was filtered and the filtrate was evaporated under reduced pressure to afford brown oil that can be directly used in the following step (7.81 g, 95%). ^{1}H NMR (400 MHz, $CDCl_3$): δ 8.03 (s, 1H), 6.92–6.94 (m, 2H), 4.60 (s, 2H), 3.54 (br s, 2H), 3.54(t, J = 6.5 Hz, 2H), 3.35 (s, 3H), 2.71 (t, J = 7.7 Hz, 2H), 1.72–1.78 (m, 2H), 1.62–1.67 (m, 2H). ^{13}C NMR (100 MHz, $CDCl_3$): δ 152.10, 140.15, 136.87, 122.63, 122.53, 96.41, 67.67, 55.11, 37.03, 29.38, 26.71.

***6-(6-(Methoxymethoxy)hexyl)pyridin-3-amine* (5b):** **5b** was prepared similarly as described for **5a** by using **4b** (10.68 g, 40.4 mmol) as the starting material. Product was obtained as brown oil (9.05 g, 94%). ^{1}H NMR (400 MHz, $CDCl_3$): δ 8.02 (m, 1H), 6.91 (m, 2H), 4.61 (s, 2H), 3.60 (br s, 2H), 3.50 (t, J = 6.6 Hz, 2H), 3.35 (s, 3H), 2.65 (t, J = 7.8 Hz, 2H), 1.64–1.71 (m, 2H), 1.55–1.60 (m, 2H), 1.35–1.41 (m, 4H). ^{13}C NMR (150 MHz, $CDCl_3$): δ 152.42, 140.13, 136.80, 122.56, 122.51, 96.39, 67.84, 55.07, 37.28, 30.10. 29.67, 29.11, 26.09.

2.1.3 | Methyl 2-((6-(4-(methoxymethoxy) butyl)pyridin-3-yl)amino)-2-methylpropanoate (7a)—Sodium acetate (30.5 g, 372 mmol) was added to a solution of **5a** (7.81 g, 37.2 mmol) and **6** (33.7 g, 186 mmol) in anhydrous ethanol (500 ml). The reaction was refluxed for 10 days. Reaction was filtered and the filtrate was concentrated under reduced pressure. The residue was diluted with EtOAc and was washed with water and brine. The organic phase was separated and dried over anhydrous Na_2SO_4 and concentrated. Crude product was purified by using flash column chromatography (Hexanes/EtOAc: 1:2 → EtOAc, 3.78 g, 34.3%). ^{1}H NMR (400 MHz, $CDCl_3$): δ 7.95 (d, J = 2.8 Hz, 1H), 6.93 (d, J = 8.4 Hz, 1H), 6.81 (dd, J = 8.4 Hz, 2.8 Hz, 1H), 4.60 (s, 2H), 4.05 (brs, 1H), 3.71 (s, 3H), 3.54 (t, J = 6.5 Hz, 2H), 3.35 (s, 3H), 2.70 (t, J = 7.6 Hz, 2H), 1.71–1.80 (m, 2H), 1.62–1.68 (m, 2H), 1.54 (s, 6H). ^{13}C NMR (100 MHz, $CDCl_3$): δ 176.18, 152.20, 139.41, 138.37, 123.11, 122.35, 96.40, 67.66, 57.73, 55.09, 52.52, 36.98, 29.41, 26.59, 26.14 (2C).

3-((4-(6-(Methoxymethoxy)hexyl)phenyl)amino)-3-methylbutan-2-one (7b): **7b** was prepared similarly as described for **7a** by using **5b** (3.0 g, 12.6 mmol) and **6** (22.8 g, 126 mmol) as the starting materials in the presence of sodium acetate (15.0 g, 189 mmol). The crude product was purified by using flash column chromatography (Hexanes/EtOAc, 1:2) to afford **7b** as yellow oil (3.1 g, 73%). ^{1}H NMR (600 MHz, $CDCl_3$): δ 7.90 (d, J = 2.8 Hz, 1H), 6.88 (d, J = 8.4 Hz, 1H), 6.78 (dd, J = 8.4Hz, 2.8 Hz, 1H), 4.56 (s, 2H), 4.00 (br s, 1H), 3.67 (s, 3H), 3.60 (t, J = 6.6 Hz, 2H), 3.46 (t, J = 6.6 Hz, 2H), 3.30 (s, 3H), 2.62 (t, J = 7.7 Hz, 2H), 1.60–1.66 (m, 2H), 1.52–1.57 (m, 2H), 1.50 (s, 6H), 1.29–1.39 (m, 4H). ^{13}C NMR (150 MHz, $CDCl_3$): δ 176.17, 152.53, 139.25, 138.21, 123.09, 122.27, 96.31, 67.76, 57.67, 55.03, 52.51, 37.18, 29.96. 29.61, 29.11, 26.09 (2C), 26.04.

4-(3-(6-(4-(Methoxymethoxy)butyl)pyridin-3-yl)-4,4-dimethyl-5-oxo-2-thioxoimidazolidin-1-yl)-2-(trifluoromethyl)benzonitrile (9a): **8** (8.78 g, 38.5 mmol) was added to a solution of **7a** (3.78 g, 12.8 mmol) in DMSO (25 ml). Reaction was stirred at 80°C overnight. The mixture was diluted with EtOAc and washed with water and brine. Organic phase was dried over anhydrous Na_2SO_4 and concentrated. The crude product was purified by using flash column chromatography (Hexanes/EtOAc: 2:1 → 1:1) to afford **9a** as brown oil (5.8 g, 90%). ^{1}H NMR (600 MHz, $CDCl_3$): δ 8.45 (d, J = 2.4 Hz, 1H), 7.96 (d, J = 8.4 Hz, 1H), 7.94 (s, 1H), 7.82 (d, J = 7.8, 1H), 7.54 (dd, J = 8.4 and 2.4 Hz, 1H), 7.33 (d, J = 8.4 Hz, 1H), 4.60 (s, 2H), 3.56 (t, J = 6.4 Hz, 2H), 3.34 (s, 3H), 2.90 (t, J = 7.8 Hz, 2H), 1.84–1.90 (m, 2H), 1.66–1.72 (m, 2H), 1.58 (s, 6H). ^{13}C NMR (150 MHz, $CDCl_3$): δ 180.32, 174.67, 163.63, 149.58, 137.44, 136.95, 135.25, 133.56 (q, J = 33.7 Hz), 132.16, 129.59, 127.04 (q, J = 4.9 Hz), 123.42, 121.82 (q, J = 274.2 Hz), 114.76, 110.24 (q, J = 2.6 Hz), 96.43, 67.43, 66.34, 55.16, 37.81, 29.44, 26.12, 23.71 (2C).

4-(3-(6-(6-(Methoxymethoxy)hexyl)pyridin-3-yl)-4,4-dimethyl-5-oxo-2-thioxoimidazolidin-1-yl)-2-(trifluoromethyl)benzonitrile (9b): **9b** was prepared similarly as described for **9a** by using **7b** (3.0 g, 8.9 mmol) and **8** (6.0 g, 26.3 mmol) as starting materials. Flash column chromatography (Hexanes/EtOAc: 1:1 → 1:2) gave **9b** as yellow oil (4.2 g, 90%). ^{1}H NMR (600 MHz, $CDCl_3$): δ 8.46 (d, J = 2.4 Hz, 1H), 7.97 (d, J = 8.3 Hz, 1H), 7.95 (d, J = 1.6 Hz, 1H), 7.83 (dd, J = 8.3 Hz, 1.9 Hz, 1H), 7.54 (dd, J = 8.2 and 2.5 Hz, 1H), 7.32 (d, J

= 8.3 Hz, 1H), 4.60 (s, 2H), 3.51 (t, *J* = 6.6 Hz, 2H), 3.34 (s, 3H), 2.87 (t, *J* = 8.0 Hz, 2H), 1.73–1.83 (m, 2H), 1.56–1.65 (m, 2H), 1.59 (s, 6H), 1.40–1.46 (m, 4H). ^{13}C NMR (150 MHz, $CDCl_3$): δ 180.33, 174.69, 164.00, 149.51, 137.42, 136.93, 135.25, 133.61 (q, *J* = 33.4 Hz), 132.14, 129.50, 127.04 (q, *J* = 4.9 Hz), 123.38, 121.81 (q, *J* = 274.3 Hz), 114.74, 110.29 (q, *J* = 2.2 Hz), 96.38, 67.71, 66.34, 55.10, 38.10, 29.60, 29.47, 29.22, 26.05, 23.73 (2C).

4-(3-(6-(4-Hydroxybutyl)pyridin-3-yl)-4,4-dimethyl-5-oxo-2-thioxoimidazolidin-1-yl)-2-(trifluoromethyl) benzonitrile (*10a*): To the solution of **9a** (5.8 g, 11.4 mmol) in methanol, hydrogen chloride (4N, in 1,4-dioxane) (15 ml, 60 mmol) was added dropwise. Reaction was stirred at room temperature overnight. Most of the solvent was removed and the residue was diluted with EtOAc and washed with saturated sodium bicarbonate. The crude product was purified by using flash column chromatography (Hexanes/EtOAc: 1:2 → 1:4 → EA) to afford **10a** as brown oil (4.9 g, 94%). ^{1}H NMR (600 MHz, $CDCl_3$): δ 8.40 (d, *J* = 1.6 Hz, 1H), 7.93 (d, *J* = 8.4 Hz, 1H), 7.92 (s, 1H), 7.80 (d, *J* = 8.4, 1H), 7.53 (dd, *J* = 8.4 and 2.2 Hz, 1H), 7.31 (d, *J* = 8.3 Hz, 1H), 3.63 (t, *J* = 6.3 Hz, 2H), 2.99 (br s, 1H), 2.86 (t, *J* = 7.8 Hz, 2H), 1.78–1.86 (m, 2H), 1.58–1.66 (m, 2H), 1.54 (s, 6H). ^{13}C NMR (150 MHz, $CDCl_3$): δ 180.3, 174.7, 163.6, 149.4, 137.7, 137.0, 135.3, 133.4 (q, *J* = 33.6 Hz), 132.3, 129.7, 127.06 (q, *J* = 5.0 Hz), 123.62, 121.84 (q, *J* = 274.3 Hz), 114.81, 110.07, 66.39, 62.02, 37.45, 32.16, 25.66, 23.62 (2C).

4-(3-(6-(6-Hydroxyhexyl)pyridin-3-yl)-4,4-dimethyl-5-oxo-2-thioxoimidazolidin-1-yl)-2-(trifluoromethyl) benzonitrile (*10b*): **10b** was prepared similarly as described for **10a**. **9b** (1.68 g, 3.14 mmol) in methanol (15 ml) was treated with hydrogen chloride (4N, in 1,4-dioxane) (4 ml). The crude product was purified by using flash column chromatography (Hexanes/EtOAc: 1:1 → 1:2) to afford **10b** as yellow foam (1.4 g, 91%). ^{1}H NMR (600 MHz, $CDCl_3$): δ 8.42 (d, *J* = 2.0 Hz, 1H), 7.93–7.95 (m, 2H), 7.81 (d, *J* = 8.2, 1H), 7.53 (dd, *J* = 8.2 and 2.0 Hz, 1H), 7.31 (d, *J* = 8.2 Hz, 1H), 3.58 (t, *J* = 6.5 Hz, 2H), 2.84 (t, *J* = 7.8 Hz, 2H), 2.16 (br s, 1H), 1.80–1.72 (m, 2H), 1.56 (s, 6H), 1.50–1.58 (m, 2H), 1.36–1.44 (m, 4H). ^{13}C NMR (150 MHz, $CDCl_3$) δ 180.33, 174.69, 163.93, 149.48, 137.51, 136.99, 135.31, 133.47 (q, *J* = 33.5 Hz), 132.19, 129.55, 127.08 (q, *J* = 5.3 Hz), 123.52, 121.83 (q, *J* = 274.26 Hz), 114.78, 110.15 (q, *J* = 2.3 Hz), 66.37, 62.59, 37.94, 32.52, 29.44, 29.04, 25.46, 23.68, 23.64. HR-ESI-MS *m*/*z* Calcd for $C_{24}H_{26}F_3N_4O_2S$ $[M + H]^+$ 491.1729, found 491.1724.

4-(3-(6-(4-Azidobutyl)pyridin-3-yl)-4,4-dimethyl-5-oxo-2-thioxoimidazolidin-1-yl)-2-(trifluoromethyl) benzonitrile (*11a*): In argon atmosphere, methanesulfonyl chloride (0.55 ml, 7.1 mmol) was added dropwise to a stirred solution of **10a** (820 mg, 1.77 mmol) in dichloromethane (DCM) and TEA (1.23 ml, 8.87 mmol) at 0°C. The resulted mixture was stirred at 0°C for 30 min and at room temperature for 1 hr. The mixture was diluted with DCM and washed with water and brine, the organic phase was separated, dried over anhydrous Na_2SO_4 and concentrated under reduced pressure. The residue was re-dissolved in DMF (15 ml), followed by the addition of sodium azide (345 mg, 5.3 mmol). The mixture was stirred at room temperature overnight and was diluted with EtOAc, washed with water and brine. The crude product was purified by using flash column chromatography (Hexanes/

EtOAc, 1:2) to afford **11a** as colorless oil (194 mg, 25%). ^{1}H NMR (600 MHz, $CDCl_3$): δ 8.48 (d, J = 2.0 Hz, 1H), 7.98 (d, J = 8.3 Hz, 1H), 7.95 (s, 1H), 7.83 (d, J = 8.2 Hz, 1H), 7.57 (dd, J = 8.2 Hz, 2.3 Hz, 1H), 7.34 (d, J = 8.2 Hz, 1H), 3.33 (t, J = 6.8 Hz, 2H), 2.91 (t, J = 7.8 Hz, 2H), 1.86–1.92 (m, 2H), 1.68–1.74 (m, 2H), 1.59 (s, 6H). ^{13}C NMR (150 MHz, $CDCl_3$): δ 180.35, 174.65, 163.09, 149.66, 137.60, 136.89, 135.26, 133.64 (q, J = 33.5 Hz), 132.13, 129.77, 127.03 (q, J = 5.1 Hz), 123.47, 121.81 (q, J = 274.5 Hz), 114.72, 110.34 (q, J = 2.6 Hz), 66.35, 51.19, 37.43, 28.51, 26.47, 23.75 (2C).

4-(3-(6-(6-Azidohexyl)pyridin-3-yl)-4,4-dimethyl-5-oxo-2-thioxoimidazolidin-1-yl)-2-(trifluoromethyl) benzonitrile (*11b*): **11b** was prepared similarly as described for **11a**. Briefly, methanesulfonate intermediate was prepared by reacting **10a** (1.35 g, 2.75 mmol) with methanesulfonyl chloride (0.42 ml, 5.47 mmol) in the presence of TEA (1.15 ml, 8.25 mmol) in DCM (15 ml) and was further converted to azide by stirring with sodium azide (506 mg, 7.8 mmol) in DMF (12 ml) at room temperature for 6 hr. Crude product was purified using flash column chromatography to give **11b** as yellow oil (1.4 g, 94%). ^{1}H NMR (600 MHz, $CDCl_3$): δ 8.45 (d, J = 2.4 Hz, 1H), 7.95 (d, J = 9.1 Hz, 1H), 7.94 (s, 1H), 7.82 (dd, J = 8.3Hz, 1.8Hz, 1H), 7.54 (dd, J = 8.2 Hz, 2.5 Hz, 1H), 7.31 (d, J = 8.3 Hz, 1H), 3.24 (t, J = 6.9 Hz, 2H), 2.85 (t, J = 7.8 Hz, 2H), 1.73–1.81 (m, 2H), 1.55–1.62 (m, 2H), 1.57 (s, 6H), 1.45–1.38 (m, 4H). ^{13}C NMR (150 MHz, $CDCl_3$): δ 180.33, 174.67, 163.77, 149.55, 137.46, 136.98, 135.26, 133.50 (q, J = 33.5 Hz), 132.19, 129.57, 127.05 (q, J = 4.9 Hz), 123.41, 121.84 (q, J = 274.2 Hz), 114.77, 110.20 (q, J = 2.3 Hz), 66.36, 51.35, 37.96, 29.27, 28.87, 28.66, 26.49, 23.68 (2C). HR-ESI-MS m/z Calcd for $C_{24}H_{25}F_3N_7OS$ $[M + H]^+$ 516.1793, found 516.1785.

4-(3-(6-(4-Isothiocyanatobutyl)pyridin-3-yl)-4,4-dimethyl-5-oxo-2-thioxoimidazolidin-1-yl)-2-(trifluoro methyl)benzonitrile (*12a*): To a solution of **11a** (194 mg, 0.40 mmol) in THF (5 ml) was added triphenylphosphine (225 mg, 0.86 mmol). The mixture was refluxed overnight, followed by the addition of carbon disulfide (3 ml) and another 12-hr reflux. Solvent was removed under reduced pressure, and the crude product was purified by using flash column chromatography (Hexanes/EtOAc, 1:1) to afford **12a** as colorless oil (53 mg, 26%). ^{1}H NMR (600 MHz, $CDCl_3$): δ 8.47 (d, J = 1.6 Hz, 1H), 7.97 (d, J = 8.3 Hz, 1H), 7.95 (s, 1H), 7.83 (d, J = 8.2 Hz, 1H), 7.57 (dd, J = 8.3 and 1.6 Hz, 1H), 7.34 (d, J = 8.2 Hz, 1H), 3.57 (t, J = 6.4 Hz, 2H), 2.90 (t, J = 7.6 Hz, 2H), 1.88–1.97 (m, 2H), 1.75–1.86 (m, 2H), 1.59 (s, 6H). ^{13}C NMR (150 MHz, $CDCl_3$): δ 180.35, 174.64, 163.66, 149.72, 137.66, 136.94, 135.28, 133.56 (q, J = 33.5 Hz), 132.18, 129.88, 127.05 (q, J = 4.9 Hz), 123.52, 121.83 (q, J = 274.3 Hz), 114.76, 110.26 (q, J = 2.4 Hz), 66.38, 44.87, 37.03, 29.52, 26.23, 23.74 (2C). ESI-MS m/z Calcd for $C_{23}H_{21}F_3N_5OS_2$ $[M + H]^+$ 504.6, found 504.3.

4-(3-(6-(6-Isothiocyanatohexyl)pyridin-3-yl)-4,4-dimethyl-5-oxo-2-thioxoimidazolidin-1-yl)-2-(trifluoro methyl)benzonitrile (*12b*): **12b** was prepared similarly as described for **12a**. Briefly, **11b** (1.5 g, 2.9 mmol) and triphenylphosphine (1.5 g, 5.8 mmol) were dissolved in THF (10 ml) and refluxed overnight followed by the addition of carbon disulfide (9 ml) and another 5-hr reflux. Solvent was removed under reduced pressure. The crude product was purified by using flash column chromatography (Hexanes/EtOAc, 1:1) to afford **12b** as yellow foam (905 mg, 59%). ^{1}H NMR (600 MHz, $CDCl_3$): δ 8.45 (d, J = 2.3 Hz, 1H), 7.96

(d, J = 8.6 Hz, 1H), 7.95 (s, 1H), 7.83 (dd, J = 8.3 Hz, 1.8Hz, 1H), 7.55 (dd, J = 8.2 Hz, 2.5 Hz, 1H), 7.32 (d, J = 8.3 Hz, 1H), 3.49 (t, J = 6.6 Hz, 2H), 2.86 (t, J = 7.9 Hz, 2H), 1.76–1.82 (m, 2H), 1.65–1.72 (m, 2H), 1.57 (s, 6H), 1.38–1.49 (m, 4H). ^{13}C NMR (150 MHz, $CDCl_3$): δ 180.33, 174.67, 163.62, 149.57, 137.52, 136.97, 135.27, 133.51 (q, J = 33.6 Hz), 132.21, 129.61, 127.06 (q, J = 5.0 Hz), 123.47, 121.84 (q, J = 274.3 Hz), 114.77, 110.20 (q, J = 2.3 Hz), 66.37, 44.97, 37.87, 29.74, 29.16, 28.50, 26.34, 23.71 (2C). HR-ESI-MS m/z Calcd for $C_{25}H_{25}F_3N_5OS_2$ $[M + H]^+$ 532.1453, found 532.1478.

N-*acetyl-S-((6-(5-(3-(4-cyano-3-(trifluoromethyl)phenyl)-5,5-dimethyl-4-oxo-2-thioxoimidazolidin-1-yl) pyridine-2-yl)hexyl)carbamothioyl)-L-cysteine* (13): To a solution of **12b** (300 mg, 0.56 mmol) in acetonitrile (3 ml) was added *N*-acetylcysteine (NAC) (60 mg, 0.37 mmol) and sodium bicarbonate (240 mg, 2.86 mmol). The reaction mixture was warmed up to about 45°C overnight with stirring. Solvent was removed under reduced pressure. The crude product was purified by using flash column chromatography (Hexanes/EtOAc, 2:1 → 1:1 → DCM/MeOH/AcOH, 10:1:1%). Purified product was re-dissolved in EtOAc and washed with distilled water to remove the remaining NAC. After concentration, **13** (**13**) was obtained as white foam (162.2 mg, 63%). ^{1}H NMR (600 MHz, $CDCl_3$) δ 8.64 (s, 1H), 8.54 (d, J = 1.8 Hz, 1H), 7.97 (d, J = 8.4 Hz, 1H), 7.94 (d, J = 1.2 Hz, 1H), 7.83 (dd, J = 8.4 Hz, 1.8 Hz, 1H), 7.67 (dd, J = 8.4 Hz, 2.4 Hz, 1H), 7.40 (d, J = 8.4 Hz, 1H), 4.70 (m, 1H), 3.35–3.99 (m, 4H), 2.86 (t, J = 7.8, 2H), 1.99 (s, 3H), 1.79–1.71 (m, 2H), 1.71–1.63 (m, 2H), 1.59 (s, 6H), 1.46–1.36 (m, 4H). ^{13}C NMR (150 MHz, $CDCl_3$) δ 196.51, 180.46, 174.58, 172.53, 171.70, 163.15, 148.45, 139.12, 136.93, 135.36, 133.53 (q, J = 33.6 Hz), 132.28, 130.35, 127.09 (q, J = 5.1 Hz), 124.30, 121.83 (q, J = 274.2 Hz), 114.77, 110.27 (q, J = 2.2 Hz), 66.50, 53.71, 47.69, 36.83, 35.67, 29.36, 28.54, 27.66, 26.20, 23.75 (2C), 22.96. HR-ESI-MS m/z Calcd for $C_{30}H_{34}F_3N_6O_4S_3$ $[M + H]^+$ 695.1756, found 695.1743.

2.2 | Molecular modeling and docking

Homology model of AR was built by using Prime (Schrödinger, LLC), in which antagonistic GR structure (PDB code: 1NHZ) was used as template (Pepe et al., 2013). The agonistic forms of AR (PDB code: 2AMB) were aligned with antagonistic GR. Docking was performed using Glide (Schrödinger, LLC) in the extra precision mode with the induced fit docking protocol. The docking site was defined by the centroid of the template ligand with a box covering the entire ligand-binding site. Coordinate files of AR, **12a**, **12b**, **13,** and Enz in pdb format are available as Supplementary Files.

2.3 | 13 releases 12b in aqueous buffer

Samples for HPLC analysis were prepared by diluting the stock solution (50 mM in DMSO) of **13** in PBS buffer (10 mM, pH 7.4) containing 5% acetonitrile. The sample for 0 min was immediately analyzed right after dilution. The aliquot of incubated samples (37°C) was analyzed at indicated time points. A linear plot of the log (peak area) versus incubation time was generated to determine the half-life ($T_{1/2}$) of decomposition. HPLC analysis was performed by using Agilent 1100 HPLC system coupled with UV-vis detector set at 260 nm. The column, mobile phase, and flow rate were described in general methods, and the gradient was as follows: t = 0 min, 10% B; t = 1 min, 10% B; t = 30 min, 90% B; 30–35 min, 90% B.

2.4 | Biological assessments

2.4.1 | Cell cultures, antibodies, and reagents—VCaP, LNCaP, C4–2, 22Rv1, RWPE-1, and MDA-kb2 cells were obtained from the American Type Culture Collection. Cells were maintained in RPMI-1640 medium (LNCaP, C4–2, 22Rv1, and VCaP) or L-15 medium (MDA-kb2) supplemented with 10% heat-inactivated fetal bovine serum (FBS) and 100 U/ml penicillin/streptomycin under 5% CO_2 at 37°C. RWPE-1 cells were maintained in Keratinocyte-SFM serum free medium supplemented with EGF (Epidermal Growth Factor) and BPE (Bovine Pituitary Extract) (Thermo Fisher, 17005042). The antibodies against acetyl-histone H3 (06–599) and acetyl-histone H4 (06–598) were purchased from Millipore Sigma-Aldrich (Burlington, MA). Acetylα-Tubulin (5335), horseradish peroxidase-conjugated anti-rabbit (7074), or anti-mouse (7076) antibodies were from Cell Signaling Technology. AR (sc-816), Hsp70 (sc-59569), Hsp90 (sc-7947), glyceraldehyde 3-phosphate dehydrogenase (sc-25778), and c-Myc (sc-40) antibodies were from Santa Cruz Biotechnology. AR-V7 antibody (AG10008) was from Precision Antibody. Luciferase assay kit (E2520) was from Promega. 5α-dihydrotestosterone (DHT) and BSO were from Sigma-Aldrich. PEITC-NAc was purchased from Santa Cruz Biotechnology. Drugs were dissolved in DMSO and freshly diluted in culture media before treatment. The final DMSO concentration was <0.1% (v/v).

2.4.2 | MTT assay—PCa cells (6×10^3 cells/well) were seeded into 96-well plate overnight and then treated with indicated compounds at indicated concentrations and time duration. MTT (3-(4, 5-Dimethylthiazol-2-yl)-2,5-diphenyltetrazolium bromide) assay was performed according to the standard protocol. Briefly, MTT (0.5 mg/ml) was incubated with cells at 37°C for 3 hr. Supernatant was removed followed by the addition of dimethyl DMSO (100 μl). After incubation for 30 min at 37°C, absorbance was read at 570 nm on a microplate reader.

2.4.3 | Luciferase assay—MDA-kb2 cells were incubated in Leibovitz's/L15 medium supplemented with 10% charcoal-stripped FBS and 1% antibiotic for 24 hr. Cells (1×10^4 cells/well) were seeded into 96-well plate for 24 hr and incubated with indicated concentration of compounds with or without DHT (1 nM) for 24 hr. For all procedure, cells were incubated at CO_2 free condition. Steady-Glo® reagent was added to culture media with shaking for 10 min. Samples (100 μl) were transferred to an opaque 96-well white plate, and luminescence was measured using a luminometer.

2.4.4 | Western Blotting—Cells treated with the indicated drug or drug combination were washed with ice-cold PBS, lysed in RIPA buffer containing 1% PMSF (phenylmethylsulphonyl fluoride, a serine protease inhibitor) for 30 min over ice and centrifuged (4°C, 8765 *g*, 15 min). The protein concentration of supernatants was determined using Pierce BCA Protein Assay Kit (Thermo Fisher, Cat# 23225). Proteins in cell lysates (~40 μg) were separated using electrophoresis on SDS-PAGE and transferred onto PVDF (polyvinylidenedifluoride) membranes. Membranes were blocked in 5% fat-free milk followed by incubation with primary antibodies overnight at 4°C, and the secondary horseradish peroxidase-conjugated anti-rabbit or anti-mouse antibodies. The blots were developed in Enhanced Chemiluminescence mixture and detected by ImageQuant™ LAS

4000 imaging system (GE). Density of protein bonds was calculated and analyzed by using imageJ software downloaded from National Institute of Health website.

2.4.5 | Colony formation assay—Cells (22Rv1 or C4–2) were seeded in six-well plates (1,000/well) and cultured overnight. Cells were then treated with **13** (1 μM in 22Rv1; 2.5 μM in C4–2), BSO (5 μM) alone or in combination for 24 hr. Cells were washed and cultured in drug-free medium (22Rv1, 11 days; C4–2, 8 days). On the last day, the medium was removed, cells were washed with PBS and fixed with methanol. The colonies were stained with crystal violet solution for 3 hr at room temperature and air-dried.

2.4.6 | Lipid peroxidation assay—Lipid peroxidation was accessed in VCaP cells using C11-BODIPY Image-iT Lipid Peroxidation Kit (C10445; Thermo Fisher Scientific). In brief, cells were plated in high-content imaging glass bottom 96-well microplates (1.5×10^4 cells/well) for 48 hr followed by the treatment of BSO (100 μM), **13** (2.5 μM) for 24 hr. Cumene hydroperoxide (CH, 100 μM, 2 hr) was used as positive control. Combinatorial treatments were conducted by pretreating cells with BSO for 16 hr, followed by **13** for 24 hr. The lipid peroxidation sensor BODIPY-C11 (10 μM) was added to the cells and incubated for 30 min followed by incubation with Hoechst 33342 (1 mM) in PBS. Cells were washed with PBS three times and fluorescence was measured using SYNERGY LX multi-mode reader (BioTek) at two wavelengths: excitation/emission of 581/590 nm for the reduced dye and the excitation/emission of 488/510 nm for the oxidized dye. The ratio of green-to-red fluorescence intensity was used as the readout of lipid peroxidation. The values were normalized to the blank negative. For live-cell imaging, the cells were treated as described above, and fluorescence images were acquired using a EVOS™ Auto 2 (Thermo Fisher Scientific) Imaging System.

2.5 | Statistical analysis

Statistical analyses were performed using GraphPad Prism 8.0. Error bars represent mean ± standard deviation (*SD*) or mean ± standard error (*SEM*) as indicated in Figure caption. The differences between data sets were compared using student's *t* test or one-way ANOVA with significance level set at $p < .05$.

3 | RESULTS

3.1 | Chemistry

3.1.1 | The design of ITC-containing AR antagonist—Several factors, such as the critical roles of AR signaling in CRPC (Tran et al., 2009), pleotropic anti-PCa activities of ITC (Novio et al., 2016) as well as the heterogenous nature of PCa tumor (Li et al., 2018), prompt us to design ITC-ARi hybrid drug that (a) competitively binds to FL AR as classical antagonist; (b) downregulates AR/AR-V to address AR overexpression and to target the constitutively active AR-V; and (c) suppresses additional PCa growth/survivial pathways, such as the elevated apoptosis threshold. The multifunctional nature of ITC-ARi could increase respond rate, cancer cell killing, and limit the drug resistance during treatment.

We selected thiohydantoin scaffold of Enz as the starting point of hybrid drug design. Enz (Figure 1a) is a FDA-approved ARi with higher AR affinity compared to the previous-generation bicalutamide (Tran et al., 2009). To specifically interact with AR, the benzonitrile ring of Enz positions inside the androgen-binding pocket and the cyano group forms essential hydrogen bonds with Arg752 and Gln711(Guo et al., 2011). As the conformationally restricted thiohydantoin ring directs the rest of the molecule to the opening side of androgen-binding cavity, the fluorobenzene ring is expected to tolerate structural modifications for hybrid drug design without losing AR affinity. In a previous study on thiohydantoin-based ARi, replacing a phenyl ring with pyridine decreased lipophilicity and improved bioavailability (Yoshino et al., 2010). We similarly changed fluorobenzene to pyridine, which lowered CLogP of **12b** compared with the fluorobenzene-based analogue (6.29 vs. 7.93, calculated by using ChemDraw 16.0). We then introduced an alkyl linker carrying ITC group to afford arylalkyl ITC and predicted that these extra structural elements can be accommodated in the space outside androgen-binding pocket. To investigate if the length of linker could impact anti-PCa activities, two ITC-ARis with four- and six-carbon chain, respectively, were prepared (**12a** and **12b**, Figure 1a). The favorable AR interactions of the designed hybrid drugs were supported by molecular docking. Because the crystal structure of antagonist-liganded AR is not available, our docking analysis was performed by using a reported homology model (Pepe et al., 2013) obtained by aligning the agonistic AR (PDB code: 2AMB) with the 3D structure of GR in its antagonistic conformation (PDB code: 1NHZ). **12a** (Figure S1a) and 12b (Figure 1b) were similarly docked at the AR LBD. Their cyano-bearing phenyl rings have almost the same binding pose to that of Enz. In all dockings, the cyano group forms hydrogen bonds with Gln711 and Arg752, respectively. The benzonitrile ring forms a T-shaped π-π interaction with Phe764. The extended structures consisting linker and ITC moiety were found to locate at a shallow surface pocket formed by Leu712, Trp741, His874, and Ile906 and do not impose steric hindrance.

N-acetyl cysteine conjugate of ITC is the ultimate in vivo metabolite of many dietary ITCs (Zhang, 2012). Moreover, NAC or cysteine conjugate of ITCs could be histone deacetylase inhibitors (HDACis) evidenced by the increased acetylation markers in cell culture and in animal models (Myzak et al., 2004, 2006). Different from common phase II drug metabolites, ITC-NAC conjugate is still biologically active (Bhattacharya et al., 2012; Hwang & Lee, 2010; Jiao et al., 1997), explained by: (a) the NAC conjugates gradually release free ITCs in biological matrix (Conaway et al., 2001); (b) Similar to ITC, ITC-NAC directly modifies protein thiols via trans-thiocarbamoylation (Shibata et al., 2011); and (c) the NAC conjugate acts as HDACi in contrast to parental ITC. **12b** was therefore converted to NAC conjugate **13** (Figure 1a). Polar NAC conjugation further reduces the CLogP of **13** to 4.92, in sharp contrast to that of **12b**. The conjugation may also avoid acute electrophilic attack to cells via gradual free ITC release. The molecular docking model predicted that the interactions of **13** with AR (Figure S1b) were similar to those of **12a** and **12b**.

3.1.2 | Synthesis of ITC-ARi 12a, 12b, and the NAC conjugate 13—

To synthesize the designed hybrid drugs, four- and six-carbon chains were firstly introduced to the pyridine ring through Sonogashira coupling (Scheme 1), respectively. The hydroxyl group of **3** was then protected as methoxy-methyl acetal (MOM) to prevent the potential

interferences in the following steps. Simultaneous hydrogenation of nitro and alkyne functionalities of **4** gave aromatic amine **5** which was alkylated by **6** in the presence of sodium acetate in ethanol. Because of the low reactivity of the aromatic amine, the reaction was refluxed for days to obtain reasonable yields. The alkylation product **7** reacted with aryl isothiocyanate **8** in DMSO at 80°C to afford the thiohydantoin **9a** and **9b** in good yields. MOM protecting group was removed by using hydrochloric acid, and the obtained free hydroxyl group was converted to azide (**11a** or **11b**) through a methanesulfonate intermediate. The transformation of azide **11** to ITC was achieved by using a one-pot two-step procedure (García-Moreno et al., 2002): triphenylphosphine reacted with the azides to generate phosphazide or iminophosphorane intermediates which further reacted with carbon disulfide (in excess) to obtain ITC-ARi **12a** and **12b**, respectively. Conjugation of **12b** with NAC in the presence of sodium bicarbonate afforded **13**.

3.1.3 | NAC conjugate 13 gradually releases free ITC 12b in aqueous solution

—*N*-acetyl cysteine conjugate of ITC reversibly forms free ITC in aqueous solution (Conaway et al., 2001). To test this possibility on the setting of ITC-ARi, we dissolved **13** (50 μM) in PBS at physiological pH (7.4) and monitored its decomposition at 37°C using HPLC. The unconjugated ITC **12b** was gradually formed (Figure 2), and the half-life of **13** was about 3.4 hr calculated based on the changes of peak area. As shown by the shorter retention time on the C18 reversed-phase HPLC column, conjugation with polar NAC notably improves polarity of **13** over **12b**. **13** therefore can be viewed as a more water soluble “prodrug” of **12b** when it is used in cell culture or administrated in vivo.

3.2 | Biological characterization

3.2.1 | ITC-ARi hybrid drugs reduce viability of PCa cells

—We firstly examined if ITC-ARi affects the viability of PCa cells. VCaP cell line naturally expresses abundant wild-type FL AR as well as AR-Vs (e.g., AR-V7) and was used as one of the cell culture models. **12a** (IC_{50} 4.85 μM) and **12b** (IC_{50} 3.89 μM) decreased viability of VCaP cells grown in full medium (Figure 3a). **12b** with longer linker showed higher potency, which is in line with the reported antiproliferative activities of phenylhexyl ITC that is either more potent or comparable to other phenylalkyl ITCs bearing shorter linkers (Sharma et al., 2008). Although milder than the free ITC **12b**, **13** (IC_{50} 6.09 μM, Figure 3a) was more potent than the NAC conjugate of PEITC (P-NAC, IC_{50} 10.13 μM, Figure 3a), a dietary arylalkyl ITC with broadly reported anticancer activities (Trachootham et al., 2006; Wang et al., 2006). Similar rank orders of potency, that is, **12b** > **13** > PEITC-NAC, were also seen in 22Rv-1 and C4–2 PCa cell lines (compared at 5 μM) (Figure 3b). Likely due to the gradually release of unconjugated **12b** to restrain abrupt electrophilic insult, **13** (2.5–10 μM) displayed better cancer selectivity of than **12b** when the two compounds were compared in PCa LNCaP cell and the non-cancerous prostatic epithelial RWPE-1 cell. In contrast to **13**, the viability of both LNCaP and RWPE-1 cells was almost equally suppressed by **12b** (Figure S2). Considering this observation together with the better water solubility, we focused on **13** for further biological characterizations.

3.2.2 | 13 inhibits dihydrotestosterone (DHT)-stimulated AR transactivation and downregulates FL AR and AR-V7

—Sustained AR signaling is one of the major

driving forces of CRPC. Derived from thiohydantoin ARi and equipped with AR-modulating ITC moiety, **13** is designed to suppress both AR transcriptional activity and the expression of AR proteins.

The impact of **13** on AR transactivation was assessed by using MDA-kb2 cell-based androgen response element (ARE) luciferase assay. MDA-kb2 cell expresses high levels of FL AR and is stably transfected with an androgen-responsive luciferase reporter plasmid, and the cellular luciferase activity is proportional to AR activation (Wilson et al., 2002). As shown in Figure 4a, DHT (1 nM) increased luciferase activity by about 8.6 fold. **13** and its precursors, that is, **10b** (an alcohol), **11b** (an azide), and **12b**, suppressed androgen stimulation in a dose-dependent manner. Although not as potent as Enz at 1 μM (60% inhibition vs. 80% inhibition), **10b** and **11b** were Enz-comparable at 2.5 and 5 μM, suggesting the novel thiohydantoin chemical scaffold retains AR antagonist activity through the direct AR interaction, and there is room for optimization in future studies. ITC hybrid drug **12b** and the NAC conjugate **13** were less effective than Enz, **10b,** and **11b** at 1 μM, but antagonized AR similarly at higher concentrations (2.5 and 5 μM). This observation can be partially explained by the electrophilicity of ITC which promotes GSH conjugation and the interactions with additional cellular proteins. **13** and **12b** showed similar AR suppression, supporting that NAC conjugate is a suitable surrogate of free ITC.

We further assessed growth inhibition of C4–2 cell line by **13** in the presence of DHT. C4–2 is a LNCaP-derived, androgen-responsive PCa cell line that is less sensitive to Enz than LNCaP and is a model to evaluate AR antagonism in CRPC setting (Lai et al., 2013). **13** (2.5 and 5 μM) was more effective than Enz in suppressing DHT (1 nM)-stimulated cell growth (Figure 4b). Considering the similar AR suppression of **13** and Enz at tested concentrations (2.5 and 5 μM) in ARE luciferase assay (Figure 4a), the effectiveness of **13** could be due to the broader impact on cell growth other than inhibiting AR pathway alone.

Sulforaphane (Gibbs et al., 2009) and PEITC (Beklemisheva et al., 2007; Wang et al., 2006) downregulate AR by inducing proteasome degradation and suppressing transcription factors (TFs) that activate *AR* gene. To investigate if ITC-ARi similarly changes AR/AR-V at protein level, VCaP cells were treated with **13** and **12b** (5 and 15 μM) for 16 hr. SFN (5 and 15 μM), Enz (10 μM), and SAHA (1 μM, a positive control for HDAC inhibition) were tested side by side for comparison. As shown in Figure 4c, 13 dose-dependently decreased both FL AR and AR-V7. It was more effective than SFN but was not as potent as **12b** at lower concentration (5 μM). Enz upregulated AR-V7 and did not change FL AR (Figure 4c). SFN was reported to elicit AR degradation via intracellularly forming HDAC6-inhibiting NAC conjugate (Gibbs et al., 2009) and HDAC6 is known to modulate AR hypersensitivity and nuclear localization in CRPC (Ai et al., 2009). To test the possible connections between ITC-ARi-caused AR downregulation and HDAC inhibition, the standard markers for HDAC6 and nuclear HDAC inhibition, that is, the acetylation of α-tubulin and histone H3, respectively, were characterized. Although SFN (15 μM) increased α-tubulin acetylation, **13** and **12b** did not show significant effects on both α-tubulin and histone H3, suggesting that HDAC inhibition may not be a critical factor in **13**/**12b**-induced AR downregulation. Besides the change of AR and AR-V, SFN, **13** and **12b** also significantly induced Hsp70 and another cellular stress marker heme oxygenase 1 (HO-1) whereas the expression of Hsp90

was not affected. These effects were further confirmed in a 12 hr time course study (Figure 4d): **13** (10 μM) induced time-dependent decline of FL AR and AR-V7, and Hsp70 and HO-1 were notably increased after 6 hr of treatment.

Full-length AR is a client protein of Hsp90 and AR-V7 might be chaperoned by other heat shock proteins (Moses et al., 2018). Because Hsp70 upregulation indicates the possible heat shock protein disruption (Kitson et al., 2013) that leads to client protein degradation, we assessed if **13** changes the stability of AR and AR-V7. VCaP cells were treated with cycloheximide (CHX, 25 μg/ml) to block new protein synthesis, and the following drug treatment significantly reduced stability of both FL AR and AR-V7 (Figure 4e). **13**-induced AR/AR-V7 downregulation was partially rescued by proteasome inhibitor MG-132 (data not shown), suggesting proteasome degradation was involved in AR reduction.

Besides the posttranslational mechanisms, suppressing TFs that drive the transcription of *AR* also leads to AR downregulation. Multiple Sp1 binding sites are located near the transcriptional initiation region of *AR* gene, and PEITC was shown to decrease AR partially through Sp1 downregulation (Beklemisheva et al., 2007; Wang et al., 2006). A recent study further shows c-Myc promotes AR-V expression by upregulating pre-mRNA splicer hnRNPA1 (Nadiminty et al., 2015). As to the ITC-ARi, the exposure of VCaP cells to **13** (5.0, 10 μM) for 24 hr dose-dependently reduced Sp1 and c-Myc at protein level (Figure 4f), suggesting **13** may additionally decrease AR through affecting relevant TFs.

3.2.3 | BSO improves anti-PCa activities of 13—GSH is the most abundant endogenous free thiol. Conjugation with GSH promotes efflux transporter-mediated export of intracellular ITC (Callaway et al., 2004). The hinderance of GSH may also interfere the interactions of ITC-GSH conjugate with relevant cellular targets. Moreover, ROS production is one of the major mechanisms of ITC-induced cancer cell death (Xiao et al., 2010) and GSH could attenuate this effect via participating various detoxification pathways as an antioxidant (Lushchak, 2012). We therefore hypothesized that depleting cellular GSH could potentiate the anticancer activities of ITC-ARi. As L-buthionine sulfoximine (BSO) is a potent and specific inhibitor of γ-glutamylcysteine ligase (γGCL), the rate-limiting enzyme of GSH biosynthesis, we combined ITC-ARi **13** with BSO and tested the combination in PCa cells.

VCaP or 22Rv1 cells were pretreated with BSO (2.5–10 μM) overnight to induce GSH deficiency, followed by **13** (1–10 μM) co-treatment for 24 hr. The combinatorial effects were quantified using “interaction index” (Falchi et al., 2017) which is defined as (% viable cells treated with drug combination)/(% viable cells treated with drug 1) × (% viable cells treated with drug 2). Synergism, antagonism, and the additive effect are characterized by an index <0.8, >1.2 and a value in between, respectively. **13** plus BSO synergistically decreased viability of both VCaP and 22Rv-1 cells (Figure 5a and Table S1). Moreover, the combination efficiently suppressed colony formation of 22Rv1 and C4–2 cells at low μM concentrations when the treated cells were cultured in drug-free media for multiple days (Figure 5b). In contrast to the synergism in PCa cells, BSO did not notably enhance the potency of **13** in non-cancerous prostatic RWPE-1 cells, even it was used at 100 μM (Figure 5c). These results suggest that **13** plus BSO might be more specific to malignant cells.

Compared to **13**, the potentiation of **11b** (an azide analogue of **13**) and PEITC-NAC by BSO were limited as shown in VCaP and 22Rv1 cells (Figure 5d), suggesting that: (a) ITC is a key mediator for potency enhancement by BSO (**13** vs. **11b**); (b) the synthetic ITC-ARi scaffold is a better carrier of ITC than PEITC (**13** vs. PEITC-NAC). The differential cellular protein binding profiles of the two compounds, such as the direct inhibitory binding of **12b**/**13** to AR, might be a main contributor for this difference. As shown in Figure 5e, 13 (2.5 μM, 16 hr) plus BSO (100 μM) efficiently downregulated AR and/or AR-V7, and upregulated HO-1 and Hsp70 in both VCaP and 22Rv-1 cells, in sharp contrast to the individual drugs alone. It is worth mentioning that 22Rv1 cell expresses high levels of AR-V7 and is resistant to Enz treatment (Li et al., 2013).

3.2.4 | 13 and BSO combination induces ferroptosis in PCa cells—Despite significantly decreasing the viability of PCa cells, the combination of **13** and BSO did not cause well detectable PARP cleavage (data not shown), indicating the activation of alternative cell death other than apoptosis. Because both ITC and BSO affect redox balance, and the upregulated HO-1 increases free intracellular ferrous iron (Fe^{2+}) via heme decomposition (Chang et al., 2018), we turned our attention to ferroptosis, a non-apoptotic cell death originated from ROS and iron-dependent oxidative lipid damage (Stockwell et al., 2017). Following this hypothesis, the dependency of viability suppression on intracellular iron and ROS was investigated. VCaP or 22Rv1 cells were pretreated with BSO (100 μM, 16 hr), followed by iron chelator DFO (100 μM) and **13** (2.5 μM in VCaP and 5 μM in 22Rv1). As expected, DFO effectively protected cells from viability loss (Figure 6a). Overexpression of HO-1 is a key mediator of ferroptosis through heme decomposition-promoted Fe^{2+} elevation. Zinc(II) protoporphyrin IX (ZnPP), a specific inhibitor of HO-1, was notably protective (Figure 6a), further supporting the involvement of iron in the growth inhibition. VCaP and 22Rv1 cells were also rescued by antioxidant α-tocopherol (α-Toc, 100 μM) and the well-recognized ferroptosis suppressor ferrostatin-1 (Fer-1, 0.5 μM) (Skouta et al., 2014; Zilka et al., 2017) (Figure 6a). Both lipophilic α-Toc and Fer-1 are able to scavenge radicals in phosphatidylcholine lipid bilayers and break the redox cycle producing lipid hydroperoxide. The protection by DFO, ZnPP, and antioxidants (α-Toc, Fer-1) supports the induction of ferroptosis by the combination of **13** and BSO. Similar rescuing effects were also observed at a much lower BSO concentration (10 μM) in VCaP and 22Rv1 cells (Figure S3), demonstrating **13** plus BSO is a robust ferroptosis-inducing modality in PCa cells. The addition of ferric ammonium citrate (FAC, 25 μM) exacerbated cell suppression of the drug combination (Figure 6b), giving another evidence supporting the iron-dependent viability suppression and the occurrence of ferroptosis. Once inside the cells, FAC (Fe^{3+}) is reduced to Fe^{2+} which makes the cells more sensitive to ferroptosis induction. In VCaP cell, although BSO alone also sensitized cells to FAC, the decrease of viability was significantly less than that of the three-reagent combination. A similar trend was also seen in C4–2 cell (Figure 6c), that is, the added ferric iron enhanced the suppressive effects of BSO (100 μM) and **13** (0.6–5 μM). Different from VCaP cells, BSO plus FAC had little impact on C4–2 cell (data not shown), likely due to the distinct nature of specific cell lines. Lipid peroxidation, the direct cause of ferroptosis, was measured by using BODIPY-C11 dye in VCaP cells. Upon oxidation in live cells, the emission of the BODIPY® 581⁄591 C11 probe shifts from red (590 nm, reduced form) to green (510 nm, oxidized form), providing a ratiometric indication

of lipid peroxidation. In contrast to vehicle and each individual treatment, **13** plus BSO markedly increased BODIPY-C11 oxidation, evidenced by the fluorescent imaging and the significantly increased 510 nm/590 nm (green/red) fluorescence ratio (Figure 6d). These results further support ferroptosis induction by the drug combination.

4 | DISCUSSION

Numerous mechanisms, such as overexpression of FL AR, upregulation of truncated AR-Vs, and apoptosis evasion are involved in the resistance of CRPC to current treatments. To address these hurdles, ITC-ARi **13** was designed as multifunctional anti-PCa agent that antagonistically binds to AR and downregulates both AR and AR-V7. Compared to **13** itself, the combination of **13** and BSO more efficiently depletes AR/AR-V7 and further induces ferroptosis in PCa cells.

Dietary ITCs are stored as inert glucosinolates in plants and are released during food consumption via plant myrosinase and/or gastrointestinal microflora-initiated decomposition cascade. ITCs are readily absorbed in vivo and are bioavailable in free or conjugated forms, such as GSH conjugate or the metabolites of mercapturic acid pathway (e.g., ITC-NAC conjugate, etc.) (Yagishita et al., 2019). Due to electrophilicity, modification of proteins is a key mechanism underlying the biological activities of ITCs. However, ITCs are differentiated from many other electrophiles by reversible covalent interactions with GSH and protein sulfhydryls (Ahn et al., 2010). The prodrug-like release and the reversible binding to cellular thiols are unique properties of dietary ITCs, which may reduce the risks associated with permanent protein modifications (Lee & Grossmann, 2012). To mimic this natural process, we converted free ITC-ARi **12b** to the NAC conjugate **13** which gradually releases **12b** in aqueous solution. The NAC conjugation not only increases polarity (Figure 2) and water solubility but also improves PCa selectivity of **13** over **12b** (Figure S2).

13 is a polypharmacological anti-PCa agent. It antagonizes DHT-stimulated AR transcriptional activity (Figure 4a) and PCa cell growth (Figure 4b), downregulates (Figure 4c,d) and decreases the stability of AR/AR-V7 (Figure 4e), and reduces c-Myc and Sp1 at protein levels (Figure 4f). The downregulation of AR, c-Myc, and Sp1 is line with the reported activities of PEITC (Wang et al., 2006) and SFN (Vyas et al., 2016). Several molecular events might be relevant to **13**-caused destabilization of AR. FL AR is a Hsp90 client protein and AR-V7 is likely chaperoned by other Hsps (Moses et al., 2018). Unliganded FL AR resides in the cytoplasm and is complexed sequentially by various Hsps (e.g., Hsp40, Hsp70, Hsp90) and co-chaperons collectively termed foldsome (Cano et al., 2013). Inhibiting Hsp90 or disrupting other foldsome members destabilizes FL AR and negatively regulates AR-Vs. For instance, besides promoting FL AR degradation, Hsp90 inhibitor onalespib also decreases AR-V7 mRNA levels through transcriptome-wide alteration of mRNA splicing (Ferraldeschi et al., 2016). Compound C86 binds to Hsp40, destabilizes both FL AR and AR-V7 and subsequently compromises their transcriptional activity (Moses et al., 2018). By using recombinant human Hsp90β as a model, studies show that several cysteine residues located at the middle domain of Hsp90 were modified by ITC or electrophilic ITC analogues. For example, SFN analogue 6-HITC was shown to covalently interact with C521 (Shibata et al., 2011) and sulfoxythiocarbamate-based SFN

analogue modifies C412, C564, and one of the vicinal C589 or C590 (Zhang et al., 2014). Because Hsp90 is a major negative regulator of heat shock factor-1 (HSF-1) and cysteine modifications cause conformational changes that hinder the chaperone function, 6-HITC and sulfoxythiocarbamates upregulated Hsp70 through HSF-1-mediated heat shock response (HSR) and destabilized Hsp90 client proteins. In our experiments, **13** decreased the stability of AR and AR-V7 and meanwhile upregulated Hsp70, suggesting that **13** may similarly affect Hsps and AR foldsome via thiocarbamoylation to accelerate the degradation of AR and AR-V. Moreover, c-Myc knockdown also compromises protein stability of FL AR and AR-V, leading to impaired AR signaling (Bai et al., 2019). From this point of view, **13**-caused c-Myc reduction (Figure 4f) could also contribute to the observed AR/AR-V7 destabilization and downregulation. As a dual-pharmacophore hybrid drug, **13** may simultaneously bind to AR and ITC-interacting proteins, whether the assumed ternary complex plays a role in FL AR destabilization is currently under investigation in our laboratory and the results will be reported accordingly. Nevertheless, we show **13** effectively decreased wild-type FL AR and AR-V7 in PCa cells. Due to the common AR/AR-V modulation by foldsome and/or c-Myc pathways, **13** might also be an effective downregulator of the mutated FL AR and other AR-V species. More studies are required to validate these speculations and to elucidate the complex mechanisms behind **13**-induced AR/AR-V7 downregulation and degradation.

13 upregulates HO-1 (Figures 4c,d and 5e), another property distinct from Enz. Studies using SFN and PEITC demonstrate ITCs upregulate HO-1 through Nrf2 activation. Human Keap 1 is a cysteine-rich protein with 27 cysteine residues. C151, surrounded by basic amino acids that lower the pKa of sulfhydryl, is particularly active and is an essential sensor of electrophilic SFN (Zhang & Hannink, 2003) and PEITC (Dayalan Naidu et al., 2018). Cysteine thiocarbamoylation of Keap1 by ITCs prevents the newly synthesized Nrf2 from being ubiquitinated by Cul3 E3 ligase, which allows Nrf2 to translocate into nucleus, heterodimerize with sMaf and initiate the transcription of detoxification/antioxidant genes, including *HO-1* and the genes encoding GSH synthesis enzymes and the Xc^- system uptaking cystine as the precursor of GSH synthesis (Zhang & Chapman, 2020). Like other ITCs, **13** may upregulate HO-1 via the interactions with the cysteine residue(s) of Keap1 and subsequently activate Nrf2. Active Nrf2 signaling is a well-recognized chemoprevention event at the tumor-initiating stage; however, its powerful cytoprotective effects could be utilized by cancer cells to enforce survival, proliferation, metastasis, and treatment resistance (Rojo de la Vega et al., 2018; Sporn & Liby, 2012). To further exploit the anti-CRPC potentials of ITC-ARi by counteracting the undesired Nrf2 adaptation, we rationally combined **13** with BSO.

Buthionine sulfoximine inhibits γ-GCL, the rate-limiting enzyme of GSH synthesis. It is relatively low toxic (Dorr et al., 1986) and has been used for the development of novel anticancer drug combinations. For example, BSO was combined with chemotherapy drug melphalan in clinical trials (O'Dwyer et al., 1996) and was administrated prior to cisplatin in animal models (Lien et al., 2016). In our study, the synergy of BSO and **13** is reflected by suppressing PCa viability (Figure 5a) and colony formation (Figure 5b), downregulating AR/AR-V and upregulating HO-1 by **13** at lower concentration (Figure 5e), as well as

inducing ferroptosis in PCa cells (Figure 6 and Figure S3). BSO could potentiate the anti-PCa activities of **13** through numerous mechanisms (Figure 7). First, because the formation of a bulky GSH conjugate hinders the interactions of ITC with their cellular targets and facilitates ITC export through cell membrane efflux pumps (Callaway et al., 2004), BSO-induced GSH deficiency could increase cellular drug accumulation and improve accessibility of **12b** or **13** to target proteins (e.g., FL AR, Keap-1), which results in efficient AR antagonism and HO-1 induction. Second, sustained HO-1 upregulation under GSH deficiency is critical for ferroptosis induction. HO-1 catalyzes the decomposition of heme into carbon monoxide, biliverdin, and Fe^{2+}, which elevates free Fe^{2+} that is a key reactant for the formation of ferroptosis-promoting lipid hydroperoxide and for Fenton reaction-originated oxidative damage (Feng & Stockwell, 2018). In our experiment, the viability of PCa cells was effectively rescued by HO-1 inhibitor ZnPP and by iron chelator DFO (Figure 6a and Figure S3), supporting the involvement of HO-1 and Fe^{2+} in ferroptosis induction. Third, BSO treatment may repress GSH-dependent cellular defense that protects cells from oxidative damage and ferroptosis induction. GSH is the reducing equivalent of glutathione peroxidase. Among them, glutathione peroxidase 4 (GPX4) is the central regulator of ferroptosis (Yang et al., 2014) and is the only known phospholipid peroxidase that converts lipid hydroperoxide to unreactive lipid alcohol. GSH deficiency may lead to insufficient lipid damage repair and the accumulation of lipid hydroperoxide. Taking together, the expanded free Fe^{2+} pool and the attenuated GSH-powered cellular defense cooperatively cause ferroptosis. Fourth, BSO counteracts GSH synthesis promoted by either drug-carried NAC or Nrf2-regulated cystine uptake. Because the decomposition of **13**–**12b**, antioxidant NAC is released either in the culture media or inside the cell. Apparently, NAC did not prevent ferroptosis induction. Possible reasons might be: (a) only low μM (e.g., 1–2.5 μM) of **13** was used in drug combination. Even fully dissociated extracellularly, the concentration is far less than the mM levels of NAC that are commonly used in various antioxidant rescue assays; (b) in the intracellular scenario, the full antioxidant potential of NAC relies on its conversion to cysteine (via enzymatic deacetylation) which further participates GSH synthesis (Rushworth & Megson, 2014). However, in the presence of BSO, NAC cannot boost GSH synthesis. Because activated Nrf2 promotes the transcription of *SLC7A11* encoding xCT (the antiporter of cystine and glutamate) and the two subunits of γGCL (i.e., GCLC and GCLM) (Okazaki et al., 2020), treating PCa cells with **13** alone may result in elevated cystine uptake and the enhanced GSH synthesis. Again, by inhibiting γGCL, BSO represses Nrf2-promoted GSH synthesis and ensures effective ferroptosis induction. Collectively, the combination of **13** and BSO reveals a pro-ferroptotic role of Nrf2 through upregulating HO-1 under GSH-deficient conditions.

Androgen receptor/AR-V are critical drivers of CRPC, however, shutting down/depleting AR signaling may not be sufficient for sustained therapeutic outcome. For instance, ADT and/or Enz provoke the overexpression of antiapoptotic proteins (Li et al., 2018; Pilling & Hwang, 2019), such as Bcl-2, Bcl-xL, and Mcl-1 that mediate apoptosis evasion and are associated with therapy resistance and disease progression. AR antagonism also enriches the AR-negative/low-AR ($AR^{-/lo}$) CRPC cells (Li et al., 2018) which are well positioned to escape from AR/AR-V-targeted therapy. From this point of view, inducing ferroptosis using the combination of ITC-ARi and BSO may provide a solution to overcome the adverse

prognostic factors associated with AR-centered treatments. Further examining ITC-ARi plus BSO in relevant models, for example, in $AR^{-/lo}$ CRPC cells, is required to clarify if the novel concept described in this work is feasible for targeting AR heterogeneity in CRPC.

In summary, we have designed ITC-ARi **13** by incorporating ITC into an AR ligand scaffold. The sulfhydryl reactivity of ITC is transiently masked as NAC conjugate which gradually releases parental ITC in aqueous solution. **13** is a single-molecule pleotropic ARi that suppresses AR at multiple levels: for example, directly binding to FL AR and downregulating AR/AR-V7 at protein level, which addresses numerous treatment-resistant mechanisms of classical ARi. Cellular anti-PCa potency of **13** is significantly enhanced by GSH synthesis inhibitor BSO. **13** and BSO cooperatively downregulate AR/AR-V and induce ferroptosis in Enz-resistant PCa cells likely through increasing the accessibility of **13/12b** to cellular targets, expanding the availability of free ferrous iron and attenuating GSH-centered cellular defense and adaptation. The synergism of **13** and BSO provides a mechanistic foundation for further studies on the combination of ITC-ARi and GSH synthesis inhibitor as innovative CRPC treatment.

Supplementary Material

Refer to Web version on PubMed Central for supplementary material.

ACKNOWLEDGMENTS

This study was supported by Department of Defense Prostate Cancer Research Program Idea Development Award W81XWH-12-1-0340 (Z.Q.), the WSU Eugene Applebaum College of Pharmacy and Health Sciences Faculty Research Award Program (Z.Q.), and the SURF (Summer Undergraduate Research Fellows) program from the Department of Pharmaceutical Sciences of WSU (K.S.).

Funding information

Wayne State University; Department of Defense Prostate Cancer Research Program

DATA AVAILABILITY STATEMENT

The data that support the findings of this study are available from the corresponding author upon reasonable request.

REFERENCES

Ahn Y-H, Hwang Y, Liu H, Wang XJ, Zhang Y, Stephenson KK, Boronina TN, Cole RN, Dinkova-Kostova AT, Talalay P, & Cole PA (2010). Electrophilic tuning of the chemoprotective natural product sulforaphane. Proceedings of the National Academy of Sciences of the United States of America, 107(21), 9590–9595. 10.1073/pnas.1004104107 [PubMed: 20439747]

Ai J, Wang Y, Dar JA, Liu J, Liu L, Nelson JB, & Wang Z (2009). HDAC6 regulates androgen receptor hypersensitivity and nuclear localization via modulating Hsp90 acetylation in castration-resistant prostate cancer. Molecular Endocrinology, 23(12), 1963–1972. 10.1210/me.2009-0188 [PubMed: 19855091]

Alumkal JJ, Slottke R, Schwartzman J, Cherala G, Munar M, Graff JN, Beer TM, Ryan CW, Koop DR, Gibbs A, Gao L, Flamiatos JF, Tucker E, Kleinschmidt R, & Mori M (2015). A phase II study of sulforaphane-rich broccoli sprout extracts in men with recurrent prostate cancer. Investigational New Drugs, 33(2), 480–489. 10.1007/s10637-014-0189-z [PubMed: 25431127]

Bai S, Cao S, Jin L, Kobelski M, Schouest B, Wang X, Ungerleider N, Baddoo M, Zhang W, Corey E, Vessella RL, Dong X, Zhang K, Yu X, Flemington EK, & Dong Y (2019). A positive role of c-Myc in regulating androgen receptor and its splice variants in prostate cancer. Oncogene, 38(25), 4977–4989. 10.1038/s41388-019-0768-8 [PubMed: 30820039]

Beklemisheva AA, Feng J, Yeh YA, Wang LG, & Chiao JW (2007). Modulating testosterone stimulated prostate growth by phenethyl isothiocyanate via Sp1 and androgen receptor down-regulation. Prostate, 67(8), 863–870. 10.1002/pros.20472 [PubMed: 17431886]

Bhattacharya A, Li Y, Geng F, Munday R, & Zhang Y (2012). The principal urinary metabolite of allyl isothiocyanate, N-acetyl-S-(N-allylthiocarbamoyl)cysteine, inhibits the growth and muscle invasion of bladder cancer. Carcinogenesis, 33(2), 394–398. 10.1093/carcin/bgr283 [PubMed: 22131350]

Callaway EC, Zhang Y, Chew W, & Chow HH (2004). Cellular accumulation of dietary anticarcinogenic isothiocyanates is followed by transporter-mediated export as dithiocarbamates. Cancer Letters, 204(1), 23–31. 10.1016/j.canlet.2003.09.021 [PubMed: 14744531]

Cano LQ, Lavery DN, & Bevan CL (2013). Mini-review: Foldosome regulation of androgen receptor action in prostate cancer. Molecular and Cellular Endocrinology, 369(1–2), 52–62. 10.1016/j.mce.2013.01.023 [PubMed: 23395916]

Chang LC, Chiang SK, Chen SE, Yu YL, Chou RH, & Chang WC (2018). Heme oxygenase-1 mediates BAY 11–7085 induced ferroptosis. Cancer Letters, 416, 124–137. 10.1016/j.canlet.2017.12.025 [PubMed: 29274359]

Conaway CC, Krzeminski J, Amin S, & Chung FL (2001). Decomposition rates of isothiocyanate conjugates determine their activity as inhibitors of cytochrome p450 enzymes. Chemical Research in Toxicology, 14(9), 1170–1176. [PubMed: 11559030]

Dayalan Naidu S, Suzuki T, Yamamoto M, Fahey JW, & Dinkova-Kostova AT (2018). Phenethyl isothiocyanate, a dual activator of transcription factors NRF2 and HSF1. Molecular Nutrition and Food Research, 62(18), e1700908. 10.1002/mnfr.201700908 [PubMed: 29710398]

Dorr RT, Liddil JD, & Soble MJ (1986). Cytotoxic effects of glutathione synthesis inhibition by L-buthionine-(SR)-sulfoximine on human and murine tumor cells. Investigational New Drugs, 4(4), 305–313. 10.1007/BF00173503 [PubMed: 3583642]

Falchi F, Giacomini E, Masini T, Boutard N, Di Ianni L, Manerba M, Farabegoli F, Rossini L, Robertson J, Minucci S, Pallavicini I, Di Stefano G, Roberti M, Pellicciari R, & Cavalli A (2017). Synthetic lethality triggered by combining olaparib with BRCA2-Rad51 disruptors. ACS Chemical Biology, 12(10), 2491–2497. 10.1021/acschembio.7b00707 [PubMed: 28841282]

Feng H, & Stockwell BR (2018). Unsolved mysteries: How does lipid peroxidation cause ferroptosis? PLoS Biology, 16(5), e2006203. 10.1371/journal.pbio.2006203 [PubMed: 29795546]

Ferraldeschi R, Welti J, Powers MV, Yuan W, Smyth T, Seed G, Riisnaes R, Hedayat S, Wang H, Crespo M, Nava Rodrigues D, Figueiredo I, Miranda S, Carreira S, Lyons JF, Sharp S, Plymate SR, Attard G, Wallis N, … de Bono JS (2016). Second-generation HSP90 inhibitor onalespib blocks mRNA splicing of androgen receptor variant 7 in prostate cancer cells. Cancer Research, 76(9), 2731–2742. 10.1158/0008-5472.CAN-15-2186 [PubMed: 27197266]

García-Moreno MI, Díaz-Pérez P, Benito JM, Ortiz Mellet C, Defaye J, & García Fernández JM (2002). One-step synthesis of non-anomeric sugar isothiocyanates from sugar azides. Carbohydrate Research, 337(21–23), 2329–2334. 10.1016/S0008-6215(02)00273-2 [PubMed: 12433497]

Gibbs A, Schwartzman J, Deng V, & Alumkal J (2009). Sulforaphane destabilizes the androgen receptor in prostate cancer cells by inactivating histone deacetylase 6. Proceedings of the National Academy of Sciences of the United States of America, 106(39), 16663–16668. 10.1073/pnas.0908908106 [PubMed: 19805354]

Guo C, Linton A, Kephart S, Ornelas M, Pairish M, Gonzalez J, Greasley S, Nagata A, Burke BJ, Edwards M, Hosea N, Kang P, Hu W, Engebretsen J, Briere D, Shi M, Gukasyan H, Richardson P, Dack K, … Fanjul AN (2011). Discovery of aryloxy tetramethylcyclobutanes as novel androgen receptor antagonists. Journal of Medicinal Chemistry, 54(21), 7693–7704. 10.1021/jm201059s [PubMed: 21936524]

Haapala K, Kuukasjarvi T, Hyytinen E, Rantala I, Helin HJ, & Koivisto PA (2007). Androgen receptor amplification is associated with increased cell proliferation in prostate cancer. Human Pathology, 38(3), 474–478. 10.1016/j.humpath.2006.09.008 [PubMed: 17217995]

Hangauer MJ, Viswanathan VS, Ryan MJ, Bole D, Eaton JK, Matov A, Galeas J, Dhruv HD, Berens ME, Schreiber SL, McCormick F, & McManus MT (2017). Drug-tolerant persister cancer cells are vulnerable to GPX4 inhibition. Nature, 551(7679), 247–250. 10.1038/nature24297 [PubMed: 29088702]

Harris WP, Mostaghel EA, Nelson PS, & Montgomery B (2009). Androgen deprivation therapy: Progress in understanding mechanisms of resistance and optimizing androgen depletion. Nature Clinical Practice Urology, 6(2), 76–85. 10.1038/ncpuro1296

Hwang ES, & Lee HJ (2010). Effects of phenylethyl isothiocyanate and its metabolite on cell-cycle arrest and apoptosis in LNCaP human prostate cancer cells. International Journal of Food Sciences and Nutrition, 61(3), 324–336. 10.3109/09637481003639092 [PubMed: 20402549]

Jiao D, Smith TJ, Yang CS, Pittman B, Desai D, Amin S, & Chung FL (1997). Chemopreventive activity of thiol conjugates of isothiocyanates for lung tumorigenesis. Carcinogenesis, 18(11), 2143–2147. 10.1093/carcin/18.11.2143 [PubMed: 9395214]

Kitson RRA, Chang C-H, Xiong R, Williams HEL, Davis AL, Lewis W, Dehn DL, Siegel D, Roe SM, Prodromou C, Ross D, & Moody CJ (2013). Synthesis of 19-substituted geldanamycins with altered conformations and their binding to heat shock protein Hsp90. Nature Chemistry, 5(4), 307–314. 10.1038/nchem.1596

Korpal M, Korn JM, Gao X, Rakiec DP, Ruddy DA, Doshi S, Yuan J, Kovats SG, Kim S, Cooke VG, Monahan JE, Stegmeier F, Roberts TM, Sellers WR, Zhou W, & Zhu P (2013). An F876L mutation in androgen receptor confers genetic and phenotypic resistance to MDV3100 (Enzalutamide). Cancer Discovery, 3(9), 1030–1043. 10.1158/2159-8290.CD-13-0142 [PubMed: 23842682]

Lai K-P, Huang C-K, Chang Y-J, Chung C-Y, Yamashita S, Li L, Lee SO, Yeh S, & Chang C (2013). New therapeutic approach to suppress castration-resistant prostate cancer using ASC-J9 via targeting androgen receptor in selective prostate cells. American Journal of Pathology, 182(2), 460–473. 10.1016/j.ajpath.2012.10.029

Lee CU, & Grossmann TN (2012). Reversible covalent inhibition of a protein target. Angewandte Chemie (International Ed. in English), 51(35), 8699–8700. 10.1002/anie.201203341 [PubMed: 22806944]

Li Q, Deng QU, Chao H-P, Liu X, Lu Y, Lin K, Liu B, Tang GW, Zhang D, Tracz A, Jeter C, Rycaj K, Calhoun-Davis T, Huang J, Rubin MA, Beltran H, Shen J, Chatta G, Puzanov I, … Tang DG (2018). Linking prostate cancer cell AR heterogeneity to distinct castration and enzalutamide responses. Nature Communications, 9(1), 3600. 10.1038/s41467-018-06067-7

Li Y, Chan SC, Brand LJ, Hwang TH, Silverstein KA, & Dehm SM (2013). Androgen receptor splice variants mediate enzalutamide resistance in castration-resistant prostate cancer cell lines. Cancer Research, 73(2), 483–489. 10.1158/0008-5472.CAN-12-3630 [PubMed: 23117885]

Lien EC, Lyssiotis CA, Juvekar A, Hu H, Asara JM, Cantley LC, & Toker A (2016). Glutathione biosynthesis is a metabolic vulnerability in PI(3)K/Akt-driven breast cancer. Nature Cell Biology, 18(5), 572–578. 10.1038/ncb3341 [PubMed: 27088857]

Lushchak VI (2012). Glutathione homeostasis and functions: Potential targets for medical interventions. Journal of Amino Acids, 2012, 736837. 10.1155/2012/736837 [PubMed: 22500213]

Mai TT, Hamaï A, Hienzsch A, Cañeque T, Müller S, Wicinski J, Cabaud O, Leroy C, David A, Acevedo V, Ryo A, Ginestier C, Birnbaum D, Charafe-Jauffret E, Codogno P, Mehrpour M, & Rodriguez R (2017). Salinomycin kills cancer stem cells by sequestering iron in lysosomes. Nature Chemistry, 9(10), 1025–1033. 10.1038/nchem.2778

McKenzie S, & Kyprianou N (2006). Apoptosis evasion: The role of survival pathways in prostate cancer progression and therapeutic resistance. Journal of Cellular Biochemistry, 97(1), 18–32. 10.1002/jcb.20634 [PubMed: 16216007]

Moses MA, Kim YS, Rivera-Marquez GM, Oshima N, Watson MJ, Beebe KE, Wells C, Lee S, Zuehlke AD, Shao H, Bingman WE, Kumar V, Malhotra SV, Weigel NL, Gestwicki JE, Trepel JB, & Neckers LM (2018). Targeting the Hsp40/Hsp70 chaperone axis as a novel strategy to treat castration-resistant prostate cancer. Cancer Research, 78(14), 4022–4035. 10.1158/0008-5472.CAN-17-3728 [PubMed: 29764864]

Myzak MC, Hardin K, Wang R, Dashwood RH, & Ho E (2006). Sulforaphane inhibits histone deacetylase activity in BPH-1, LNCaP and PC-3 prostate epithelial cells. Carcinogenesis, 27(4), 811–819. 10.1093/carcin/bgi265 [PubMed: 16280330]

Myzak MC, Karplus PA, Chung FL, & Dashwood RH (2004). A novel mechanism of chemoprotection by sulforaphane: Inhibition of histone deacetylase. Cancer Research, 64(16), 5767–5774. 10.1158/0008-5472.CAN-04-1326 [PubMed: 15313918]

Nadiminty N, Tummala R, Liu C, Lou W, Evans CP, & Gao AC (2015). NF-kappaB2/p52:C-Myc:hnRNPA1 pathway regulates expression of androgen receptor splice variants and enzalutamide sensitivity in prostate cancer. Molecular Cancer Therapeutics, 14(8), 1884–1895. 10.1158/1535-7163.MCT-14-1057 [PubMed: 26056150]

Novio S, Cartea ME, Soengas P, Freire-Garabal M, & Nunez-Iglesias MJ (2016). Effects of brassicaceae isothiocyanates on prostate cancer. Molecules, 21(5), 626. 10.3390/molecules21050626

O'Dwyer PJ, Hamilton TC, LaCreta FP, Gallo JM, Kilpatrick D, Halbherr T, Brennan J, Bookman MA, Hoffman J, Young RC, Comis RL, & Ozols RF (1996). Phase I trial of buthionine sulfoximine in combination with melphalan in patients with cancer. Journal of Clinical Oncology, 14(1), 249–256. 10.1200/JCO.1996.14.1.249 [PubMed: 8558205]

Okazaki K, Papagiannakopoulos T, & Motohashi H (2020). Metabolic features of cancer cells in NRF2 addiction status. Biophysical Reviews, 12(2), 435–441. 10.1007/s12551-020-00659-8 [PubMed: 32112372]

Ou S, Xu L, & Qin Z (2017). Synthesis and In vitro anti-prostate cancer activities of androgen receptor ligand-isothiocyanate hybrid drug. Proceedings of the AACR-NCI-EORTC International Conference: Molecular Targets and Cancer Therapeutics; 2017 Oct 26–30; Philadelphia, PA. Philadelphia (PA). Mol Cancer Ther 2018;17(1 Suppl): Abstract nr A197.

Pepe A, Pamment M, Kim YS, Lee S, Lee MJ, Beebe K, Filikov A, Neckers L, Trepel JB, & Malhotra SV (2013). Synthesis and structure-activity relationship studies of novel dihydropyridones as androgen receptor modulators. Journal of Medicinal Chemistry, 56(21), 8280–8297. 10.1021/jm301714s [PubMed: 24044500]

Pilling AB, & Hwang C (2019). Targeting prosurvival BCL2 signaling through Akt blockade sensitizes castration-resistant prostate cancer cells to enzalutamide. Prostate, 79(11), 1347–1359. 10.1002/pros.23843 [PubMed: 31228231]

Qin Z, Xu L, & Ou S (2019). Isothiocyanate-containing hybrid androgen receptor (AR) antagonist downregulates AR and induces ferroptosis in GSH–deficient prostate cancer cells. AACR-NCI-EORTC International Conference on Molecular Targets and Cancer Therapeutics, October 26–30, Boston, MA. Mol Cancer Ther 2019;18 (12 Suppl): Abstract nr A110.

Rojo de la Vega M, Chapman E, & Zhang DD (2018). NRF2 and the hallmarks of cancer. Cancer Cell, 34(1), 21–43. 10.1016/j.ccell.2018.03.022 [PubMed: 29731393]

Rushworth GF, & Megson IL (2014). Existing and potential therapeutic uses for N-acetylcysteine: The need for conversion to intracellular glutathione for antioxidant benefits. Pharmacology and Therapeutics, 141(2), 150–159. 10.1016/j.pharmthera.2013.09.006 [PubMed: 24080471]

Sharma AK, Sharma A, Desai D, Madhunapantula SV, Huh SJ, Robertson GP, & Amin S (2008). Synthesis and anticancer activity comparison of phenylalkyl isoselenocyanates with corresponding naturally occurring and synthetic isothiocyanates. Journal of Medicinal Chemistry, 51(24), 7820–7826. 10.1021/jm800993r [PubMed: 19053750]

Shibata T, Kimura Y, Mukai A, Mori H, Ito S, Asaka Y, Oe S, Tanaka H, Takahashi T, & Uchida K (2011). Transthiocarbamoylation of proteins by thiolated isothiocyanates. Journal of Biological Chemistry, 286(49), 42150–42161. 10.1074/jbc.M111.308049

Skouta R, Dixon SJ, Wang J, Dunn DE, Orman M, Shimada K, Rosenberg PA, Lo DC, Weinberg JM, Linkermann A, & Stockwell BR (2014). Ferrostatins inhibit oxidative lipid damage and cell death in diverse disease models. Journal of the American Chemical Society, 136(12), 4551–4556. 10.1021/ja411006a [PubMed: 24592866]

Sporn MB, & Liby KT (2012). NRF2 and cancer: The good, the bad and the importance of context. Nature Reviews Cancer, 12(8), 564–571. 10.1038/nrc3278 [PubMed: 22810811]

Stockwell BR, Friedmann Angeli JP, Bayir H, Bush AI, Conrad M, Dixon SJ, Fulda S, Gascón S, Hatzios SK, Kagan VE, Noel K, Jiang X, Linkermann A, Murphy ME, Overholtzer M, Oyagi A, Pagnussat GC, Park J, Ran Q, … Zhang DD (2017). Ferroptosis: A regulated cell death nexus linking metabolism, redox biology, and disease. Cell, 171(2), 273–285. 10.1016/j.cell.2017.09.021 [PubMed: 28985560]

Trachootham D, Zhou Y, Zhang H, Demizu Y, Chen Z, Pelicano H, Chiao PJ, Achanta G, Arlinghaus RB, Liu J, & Huang P (2006). Selective killing of oncogenically transformed cells through a ROS-mediated mechanism by beta-phenylethyl isothiocyanate. Cancer Cell, 10(3), 241–252. 10.1016/j.ccr.2006.08.009 [PubMed: 16959615]

Traka MH, Melchini A, & Mithen RF (2014). Sulforaphane and prostate cancer interception. Drug Discovery Today, 19(9), 1488–1492. 10.1016/j.drudis.2014.07.007 [PubMed: 25051139]

Tran C, Ouk S, Clegg NJ, Chen Y, Watson PA, Arora V, Wongvipat J, Smith-Jones PM, Yoo D, Kwon A, Wasielewska T, Welsbie D, Chen CD, Higano CS, Beer TM, Hung DT, Scher HI, Jung ME, & Sawyers CL (2009). Development of a second-generation antiandrogen for treatment of advanced prostate cancer. Science, 324(5928), 787–790. 10.1126/science.1168175 [PubMed: 19359544]

Viswanathan VS, Ryan MJ, Dhruv HD, Gill S, Eichhoff OM, Seashore-Ludlow B, Kaffenberger SD, Eaton JK, Shimada K, Aguirre AJ, Viswanathan SR, Chattopadhyay S, Tamayo P, Yang WS, Rees MG, Chen S, Boskovic ZV, Javaid S, Huang C, … Schreiber SL (2017). Dependency of a therapy-resistant state of cancer cells on a lipid peroxidase pathway. Nature, 547(7664), 453–457. 10.1038/nature23007 [PubMed: 28678785]

Vyas AR, Moura MB, Hahm ER, Singh KB, & Singh SV (2016). Sulforaphane Inhibits c-Myc-mediated prostate cancer stem-like traits. Journal of Cellular Biochemistry, 117(11), 2482–2495. 10.1002/jcb.25541 [PubMed: 26990292]

Wang LG, Liu XM, & Chiao JW (2006). Repression of androgen receptor in prostate cancer cells by phenethyl isothiocyanate. Carcinogenesis, 27(10), 2124–2132. 10.1093/carcin/bgl075 [PubMed: 16704988]

Wilson VS, Bobseine K, Lambright CR, & Gray LE Jr (2002). A novel cell line, MDA-kb2, that stably expresses an androgen- and glucocorticoid-responsive reporter for the detection of hormone receptor agonists and antagonists. Toxicological Sciences, 66(1), 69–81. 10.1093/toxsci/66.1.69 [PubMed: 11861974]

Xiao D, Powolny AA, Moura MB, Kelley EE, Bommareddy A, Kim S-H, Hahm E-R, Normolle D, Van Houten B, & Singh SV (2010). Phenethyl isothiocyanate inhibits oxidative phosphorylation to trigger reactive oxygen species-mediated death of human prostate cancer cells. Journal of Biological Chemistry, 285(34), 26558–26569. 10.1074/jbc.M109.063255

Yagishita Y, Fahey JW, Dinkova-Kostova AT, & Kensler TW (2019). Broccoli or sulforaphane: Is it the source or dose that matters? Molecules, 24(19), 10.3390/molecules24193593

Yang WS, SriRamaratnam R, Welsch ME, Shimada K, Skouta R, Viswanathan VS, Cheah JH, Clemons PA, Shamji AF, Clish CB, Brown LM, Girotti AW, Cornish VW, Schreiber SL, & Stockwell BR (2014). Regulation of ferroptotic cancer cell death by GPX4. Cell, 156(1–2), 317–331. 10.1016/j.cell.2013.12.010 [PubMed: 24439385]

Yoshino H, Sato H, Shiraishi T, Tachibana K, Emura T, Honma A, Ishikura N, Tsunenari T, Watanabe M, Nishimoto A, Nakamura R, Nakagawa T, Ohta M, Takata N, Furumoto K, Kimura K, & Kawata H (2010). Design and synthesis of an androgen receptor pure antagonist (CH5137291) for the treatment of castration-resistant prostate cancer. Bioorganic and Medicinal Chemistry, 18(23), 8150–8157. 10.1016/j.bmc.2010.10.023 [PubMed: 21050768]

Zhang DD, & Chapman E (2020). The role of natural products in revealing NRF2 function. Natural Products Reports, 37(6), 797–826. 10.1039/c9np00061e

Zhang DD, & Hannink M (2003). Distinct cysteine residues in Keap1 are required for Keap1-dependent ubiquitination of Nrf2 and for stabilization of Nrf2 by chemopreventive agents and oxidative stress. Molecular and Cellular Biology, 23(22), 8137–8151. 10.1128/mcb.23.22.8137-8151.2003 [PubMed: 14585973]

Zhang Y (2012). The molecular basis that unifies the metabolism, cellular uptake and chemopreventive activities of dietary isothiocyanates. Carcinogenesis, 33(1), 2–9. 10.1093/carcin/bgr255 [PubMed: 22080571]

Zhang Y, Dayalan Naidu S, Samarasinghe K, Van Hecke GC, Pheely A, Boronina TN, Cole RN, Benjamin IJ, Cole PA, Ahn Y-H, & Dinkova-Kostova AT (2014). Sulphoxythiocarbamates modify cysteine residues in HSP90 causing degradation of client proteins and inhibition of cancer cell proliferation. British Journal of Cancer, 110(1), 71–82. 10.1038/bjc.2013.710 [PubMed: 24322890]

Zhang Y, Tan H, Daniels JD, Zandkarimi F, Liu H, Brown LM, Uchida K, O'Connor OA, & Stockwell BR (2019). Imidazole ketone erastin induces ferroptosis and slows tumor growth in a mouse lymphoma model. Cell Chemical Biology, 26(5), 623–633. 10.1016/j.chembiol.2019.01.008 [PubMed: 30799221]

Zilka O, Shah R, Li B, Friedmann Angeli JP, Griesser M, Conrad M, & Pratt DA (2017). On the mechanism of cytoprotection by ferrostatin-1 and liproxstatin-1 and the role of lipid peroxidation in ferroptotic cell death. ACS Central Science, 3(3), 232–243. 10.1021/acscentsci.7b00028 [PubMed: 28386601]

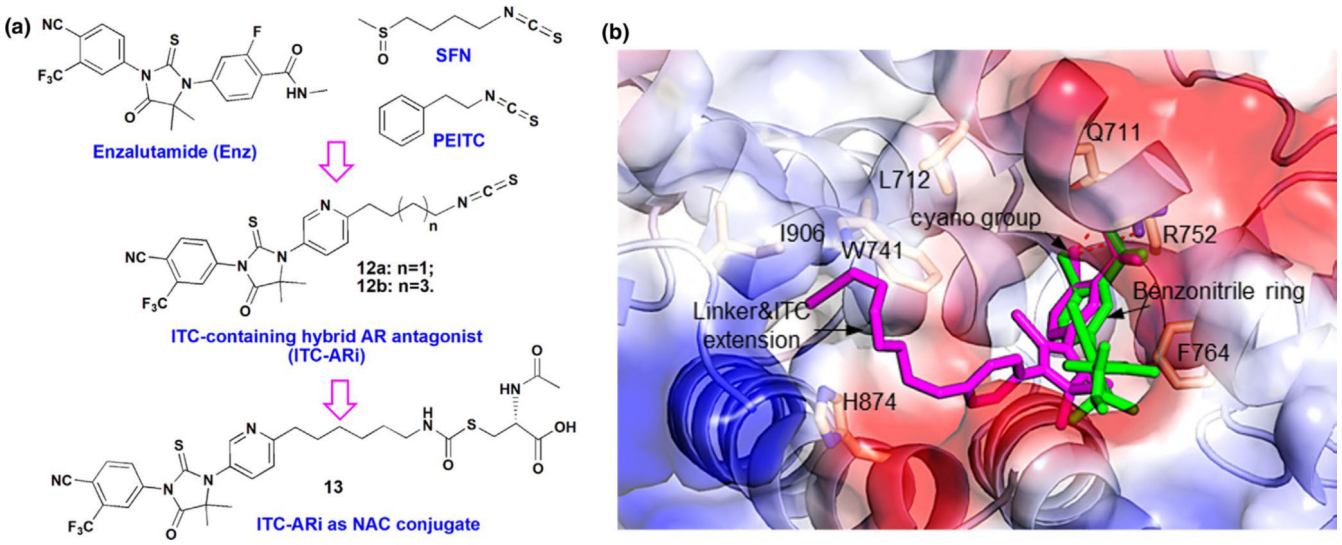

FIGURE 1.

Design of ITC-containing AR antagonist. (a) Chemical structures of enzalutamide (Enz), sulforaphane (SFN), phenethyl isothiocyanate (PEITC), and ITC-containing AR antagonists (ITC-ARi) **12a**, **12b,** and **13**. (b) The predicted interactions of **12b** and Enz with AR. Homology model was constructed by aligning the agonistic form of AR (PDB: 2AMB) with glucocorticoid receptor (GR) antagonistic conformation (PDB: 1NHZ) (Pepe et al., 2013). Docked **12b** and Enz are colored in magenta and green, respectively. AR residues involved in drug interactions are depicted as yellow sticks. Dashed lines indicate hydrogen bonds

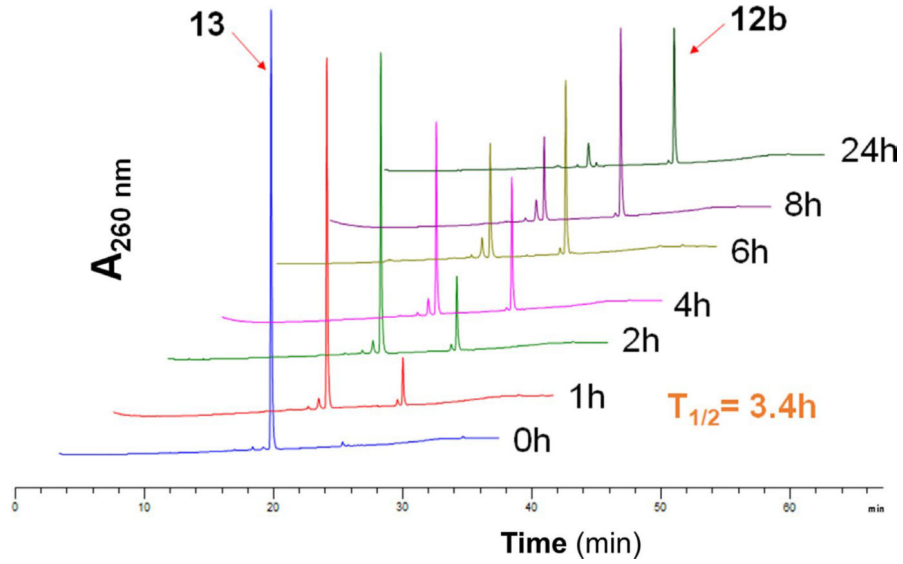

FIGURE 2.

N-acetyl cysteine conjugate **13** releases ITC-ARi 12b in aqueous solution. **13** (50 μM) was dissolved in PBS buffer (pH 7.4, 5% acetonitrile) and incubated at 37°C. Aliquots (10 μl) were taken at indicated time points and analyzed using high-performance liquid chromatography

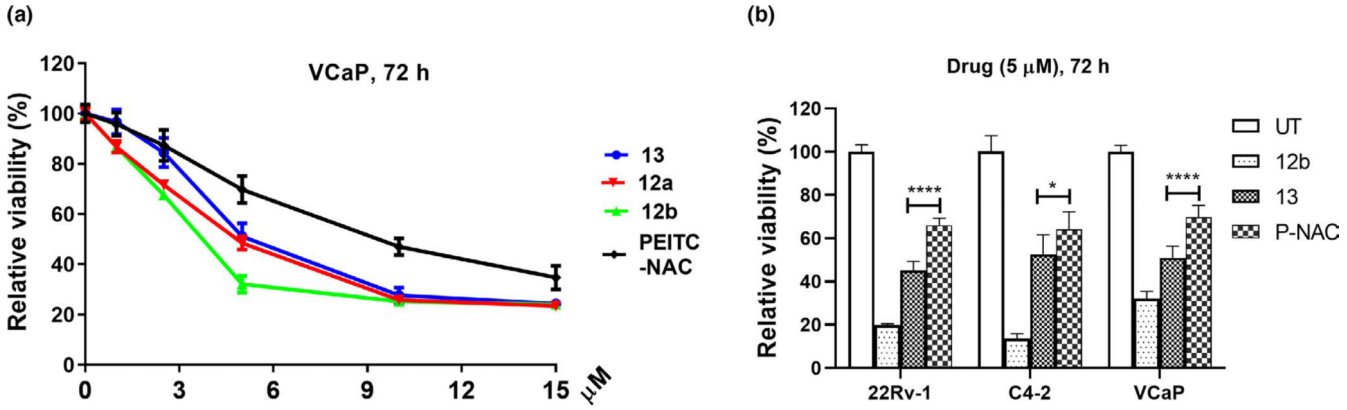

FIGURE 3.

Isothiocyanate-ARi hybrid drugs reduce viability of PCa cells. (a) VCaP cells were treated with indicated compounds at various concentrations for 72 hr. Data were plotted as means ± *SEM* (n = 6–8). (b) 22Rv1, C4–2, and VCaP cells were treated with indicated compounds at 5 μM for 72 hr. Data represent mean ± *SD* (n = 6–8). Cell viability was measured using MTT assay. *p < .05; ****p < .0001. P-NAC, NAC conjugate of PEITC

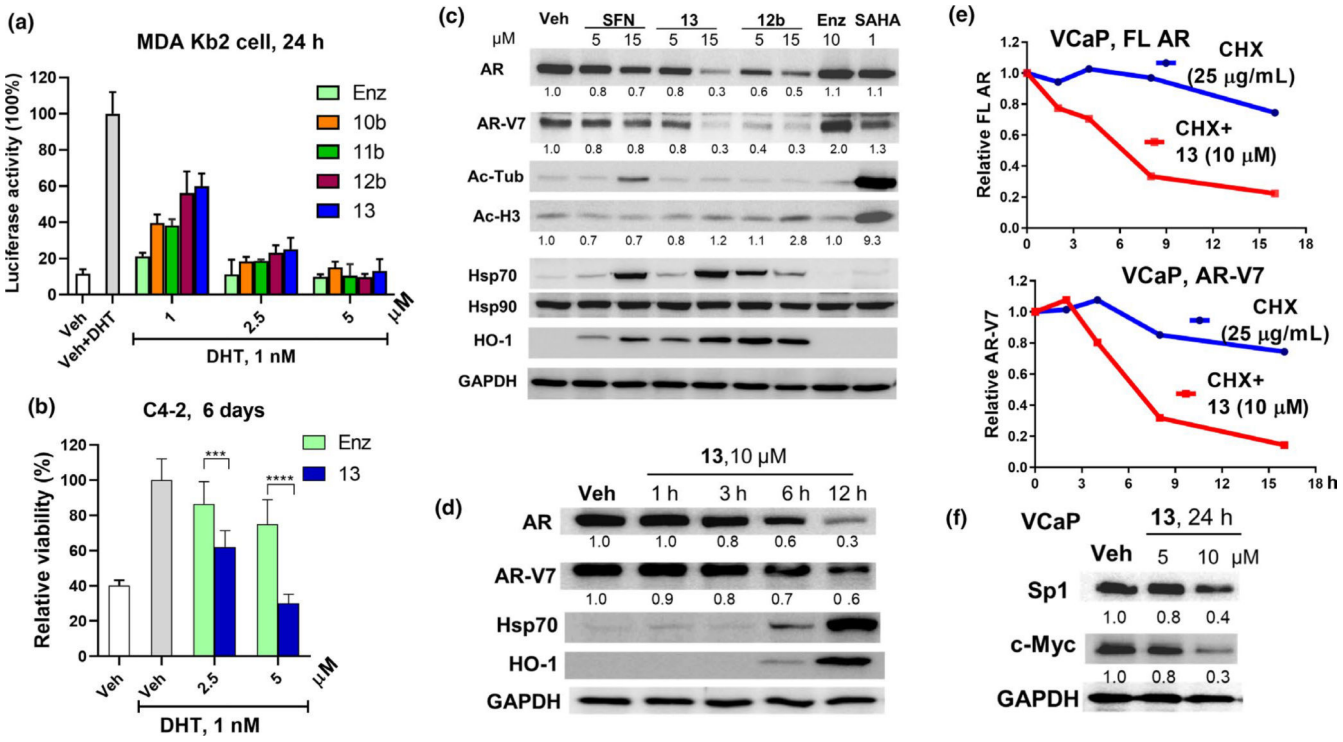

FIGURE 4.

13 induces AR antagonism in PCa cells. (a) **13** inhibits DHT (1 nM)-stimulated AR transcriptional activity in MDA-kb2 cells. Cells were cultured in Leibovitz's/L15 medium supplemented with charcoal-stripped FBS (10%) and were treated with drugs and DHT at indicated concentrations for 24 hr. Data reflect mean ± *SD* (*n* = 4). (b) C4–2 cells were cultured in RPMI-1640 medium supplemented with charcoal-stripped FBS (10%) and were treated with Enz and **13** at 2.5 and 5 μM in the presence of DHT (1 nM) for 6 days. Medium and drugs were refreshed every 2 days. Bars represent mean ± *SD* (*n* = 6–8). ****p* < .001; *****p* < .0001. (c) **13** downregulates FL AR and AR-V7. VCaP cells were treated with **13**, **12b**, SFN, Enz, and SAHA at indicated concentrations for 16 hr. Whole-cell lysates were subjected to Western blotting and probed with the indicated antibodies. (d) VCaP cells were treated with **13** (10 μM) for indicated time. AR, AR-V7, Hsp70, and HO-1 were analyzed using Western blotting and densitometry. (e) **13** reduces the stability of FL AR and AR-V7. VCaP cells were treated with cycloheximide (CHX, 25 μg/ml) in the absence or presence of **13** (10 μM). AR and AR-V7 proteins were analyzed using Western blotting and densitometry at indicated time points (2, 4, 8, 16 hr). (f) **13** downregulates transcription factors Sp1 and c-Myc. VCaP cells were treated with **13** at 5 or 10 μM for 24 hr. Sp1 and c-Myc proteins were analyzed using Western blotting. Representative images of Western blotting analysis are shown in c, d, and f. Relative expression levels normalized against GAPDH are indicated under blots. Veh, Vehicle; GAPDH, glyceraldehyde 3-phosphate dehydrogenase

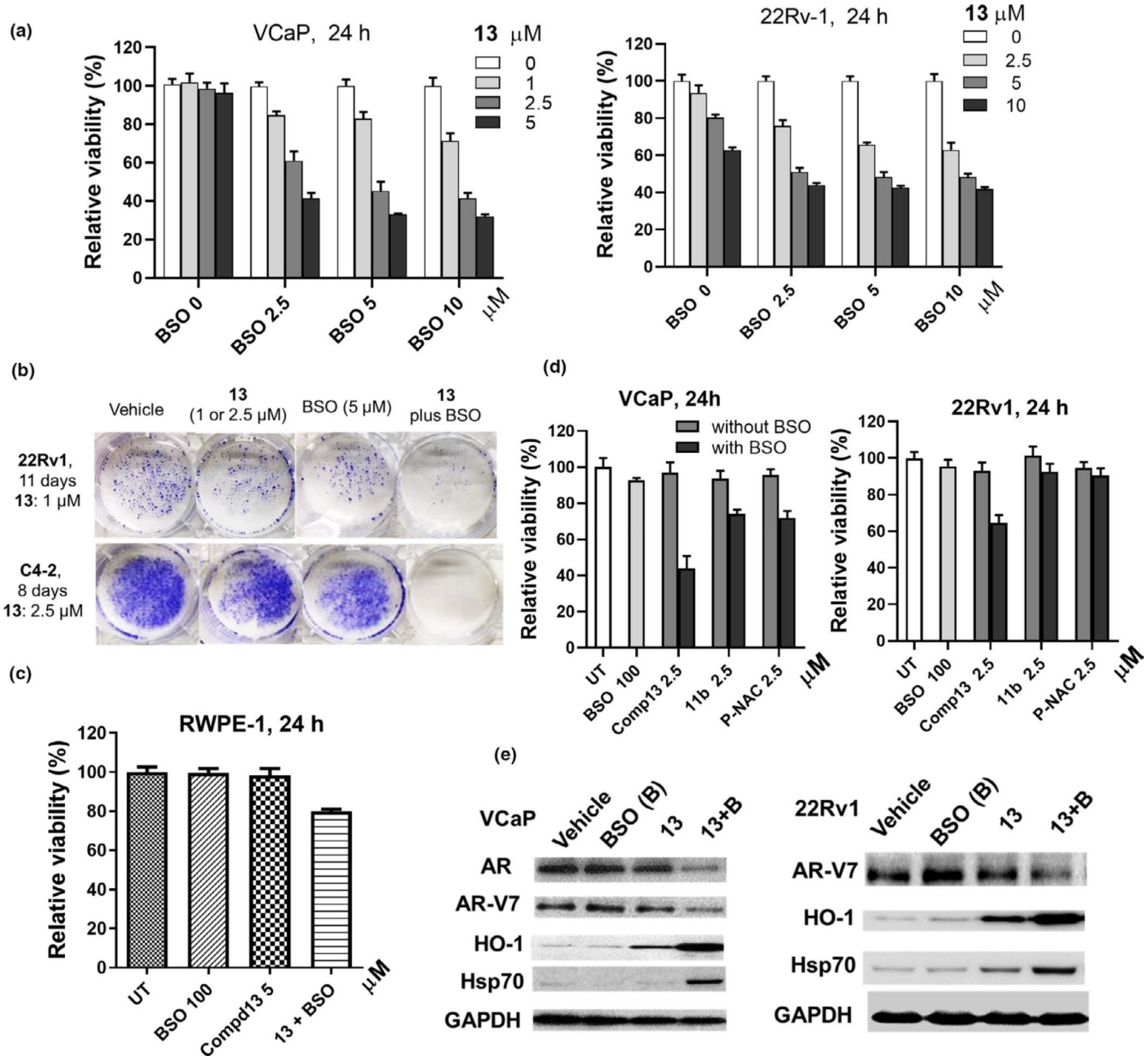

FIGURE 5.

Buthionine sulfoximine (BSO) improves anti-PCa activities of **13**. Combinatorial treatments were conducted by pretreating cells with BSO for 16 hr, followed by drugs (**13**, **11b** or PEITC-NAC) for 24 hr at indicated concentrations. Viability was measured using MTT assay (n = 6–8) in a, c, and d, data reflect mean ± *SD*. (a) **13** (1–5 μM) plus BSO (2.5–10 μM) synergistically reduced viability of VCaP cells and 22Rv-1 cells. (b) **13** (1 μM in 22Rv1; 2.5 μM in C4–2) plus BSO (5 μM) combination effectively inhibits colony formation of C4–2 and 22Rv1 cells (1,000 cell/well). Cells were treated for 24 hr and then were grown in drug-free media. (c) Non-cancerous RWPE-1 cells are much less affected by drug combination. (d) **13** is a better "carrier" of ITC. (e) **13** plus BSO effectively downregulates AR or AR-V7 and upregulates HO-1 and Hsp70. VCaP or 22Rv-1 cells were pretreated with

BSO (100 μM) for 6 hr followed by **13** (2.5 μM) co-treatment for 16 hr. Indicated proteins and GAPDH (loading control) were analyzed using Western blotting. Representative images are shown. P-NAC, PEITC-NAC

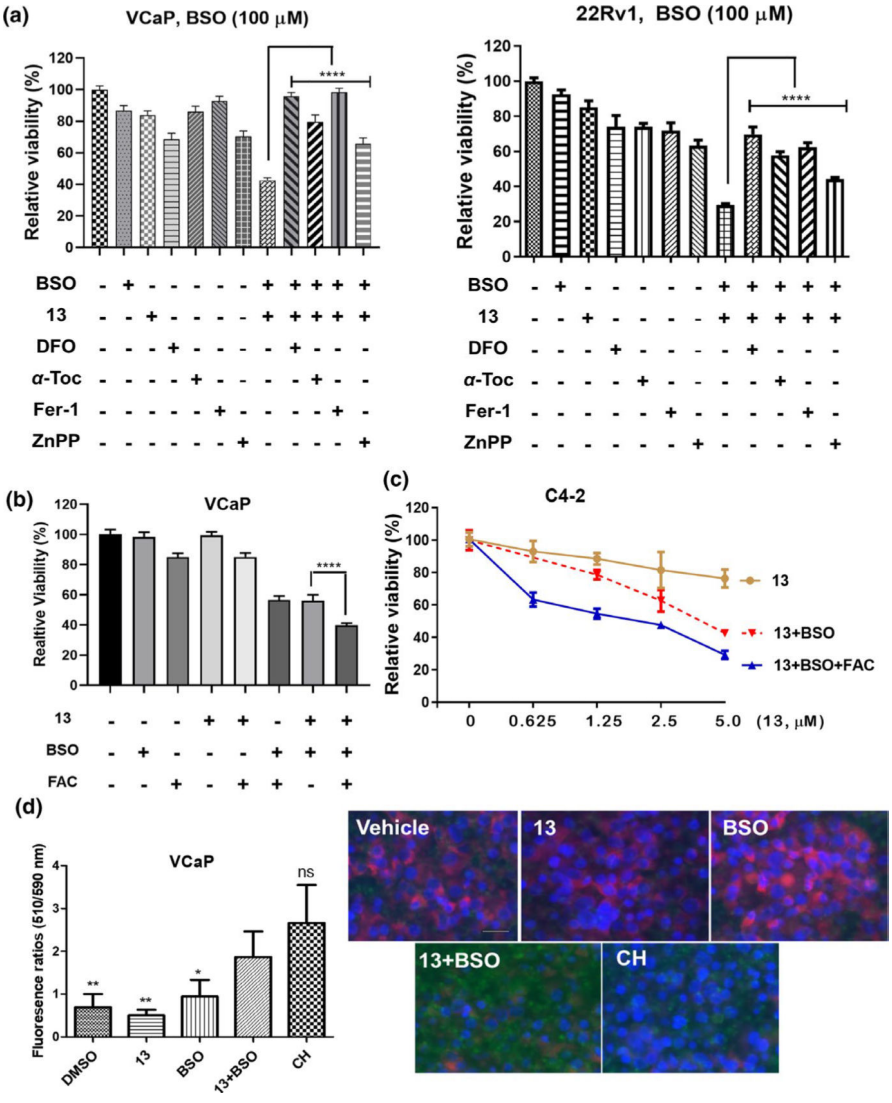

FIGURE 6.

13 and buthionine sulfoximine (BSO) combination induces ferroptosis in PCa cells. (a) **13** plus BSO-caused viability suppression is rescued by antioxidants, iron chelator, and HO-1 inhibitor. VCaP or 22Rv1 cells were treated with **13** (VCaP, 2.5 μM; 22Rv1, 5 μM), DFO (100 μM), α-Tocopherol (α-Toc, 100 μM), ferrostatin-1 (Fer-1, 0.5 μM), or ZnPP (3 μM) individually or in combination for 24 hr. BSO (100 μM) was added 16 hr prior to other agents. Values stand for mean ± *SD* (*n* = 6–8). ****$p < .0001$. (b, c) Exogenous iron enhances the potency of **13** plus BSO. VCaP cells were treated with **13** (1 μM), BSO (100 μM), and FAC (25 μM) individually or in combination for 24 hr. BSO was added 16 hr prior to other agents (b). Values stand for mean ± *SD* (*n* = 6–8), ****$p < .0001$. Similarly, C4–2 cells were treated by **13** (0.6–5 μM) or its combination with BSO (100 μM) and FAC (25 μM). BSO was added 16 hr prior to other agents (c). Data were plotted as mean ± *SD* (*n* = 6–8). Viability was assessed using MTT assay. FAC, ferric ammonium citrate. (d) Combination of **13** and BSO increased lipid peroxidation in VCaP cells. Cells were incubated with CH (100 μM, positive control) for 2 hr, BSO (100 μM) or **13** (2.5 μM) for 24

hr. Combinatorial treatments were conducted by pretreating cells with BSO for 16 hr, followed by **13** for 24 hr. Lipid peroxidation was characterized as the ratio (left) of fluorescence emission at 510 nm and 590 nm using BODIPY-C11 fluorescent reporter. Data were plotted as mean ± *SD* ($n = 5$), *$p < .05$, **$p < .01$ versus **13** and BSO combination. Fluorescence images of the treated cells were shown on the right. Cell nuclei were stained with Hoechst 33342 in blue. Scale bar, 25 μm

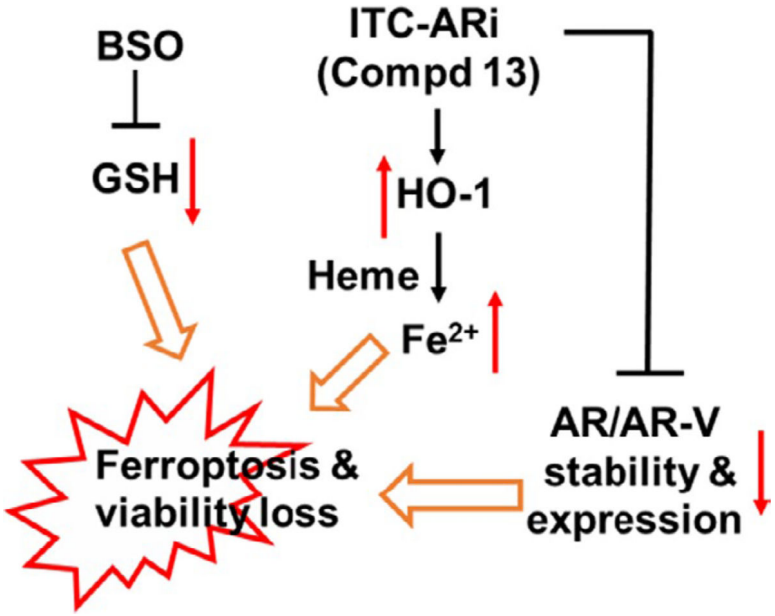

FIGURE 7.

Isothiocyanate (ITC)-ARi and BSO cooperatively induce ferroptosis and downregulates AR/AR-V in PCa cells. BSO-induced GSH deficiency enhances the anti-PCa activities of ITC-ARi and attenuates GSH-centered cellular defense

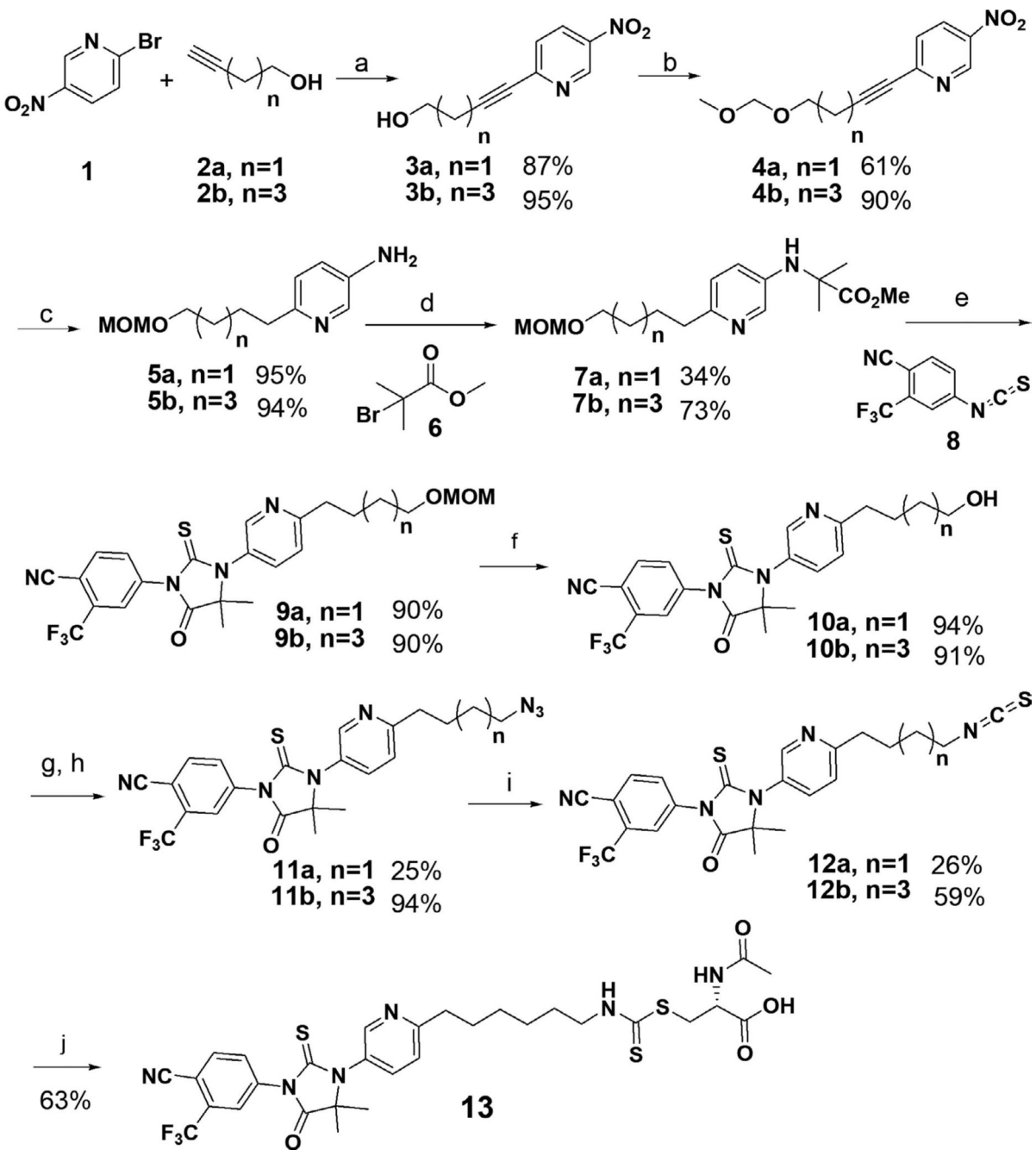

SCHEME 1.

Synthesis of isothiocyanate (ITC)-containing AR antagonists **12a**, **12b**, and NAC conjugate **13**. Reagents and conditions: (a) CuI, $Pd(PPh_3)_2Cl_2$, TEA, CH_3CN, r.t., 2 hr; (b) DIPEA, MOMBr, THF, r.t., 6 hr; (c) H_2, Pd/C, r.t., overnight. (d) NaOAc, EtOH, reflux, 10 days; (e) DMSO, 80°C, overnight; (f) HCl, MeOH, 3 hr; (g) TEA, MsCl, DCM, r.t., 30 min; (h) NaN_3, DMF, r.t., 6 hr; (i) 1. PPh_3, THF, reflux, overnight; 2.CS_2, THF, reflux, 5 hr; (j) NAC, $NaHCO_3$, acetonitrile, 45°C, overnight